Cross-kingdom conservation of Arabidopsis RPS24 function in 18S rRNA maturation

Adrián Cabezas-Fuster, Rosa Micol-Ponce, Raquel Sarmiento-Mañús, and María Rosa Ponce

Instituto de Bioingeniería, Universidad Miguel Hernández, Campus de Elche, 03202 Elche, Alicante, Spain.

Running title: RPS24A and RPS24B function in 18S rRNA maturation

Corresponding author: María Rosa Ponce (telephone: +34 96 665 8503; fax: +34 96 665 8511; e-mail: mrponce@umh.es)

ABSTRACT

All 81 ribosomal proteins (RPs) that form the Arabidopsis (*Arabidopsis thaliana*) 80S ribosome are encoded by several paralogous genes. For example, the nearly identical RPS24A and RPS24B proteins are encoded by *RPS24A* and *RPS24B*, respectively. Here we explored the functions of RPS24A and RPS24B in Arabidopsis. Their encoding genes exhibit combined haploinsufficiency, as at least two wild-type copies of either *RPS24A* or *RPS24B* are required for plant viability and at least three are required for normal plant development. Loss-of-function of either gene caused a pointed-leaf phenotype, a typical phenotype of null or hypomorphic recessive alleles of genes encoding ribosome biogenesis factors (RBFs) or RPs. We also found that RPS24A and RPS24B act as RBFs during early stages of 18S ribosomal RNA (rRNA) maturation, as loss of RPS24A or RPS24B function reduced the 18S/25S rRNA ratio. An RPS24B-GFP fusion protein predominantly localized to the nucleolus, as expected. The *rps24b-2* mutation strengthened the phenotypes of the RBF mutants *mRNA transporter4-2* and *small organ4-3*, which are defective in 5.8S rRNA maturation. This synergistic interaction might be an effect of increased 45S rDNA transcription, which we also observed in the *rps24* mutants. Therefore, the Arabidopsis RPS24 proteins act as RBFs during 18S rRNA maturation, like their human and yeast putative orthologs. Only two plant RPs were previously shown to act not only as structural components of the ribosome but also as RBFs. We provide evidence that RPS24 proteins also regulate 45S rDNA transcription, which has not been described for their yeast or human orthologs.

KEYWORDS

RPS24; ribosome biogenesis; Arabidopsis; pre-rRNA processing; 45S rDNA expression, 18S rRNA maturation.

INTRODUCTION

The 80S cytoplasmic ribosome (hereafter, the ribosome) of Arabidopsis (*Arabidopsis thaliana*) is composed of four ribosomal RNAs (rRNAs) and 81 ribosomal proteins (RPs; Wilson and Cate, 2012), consisting of 33 RPs in its small (40S) subunit and 48 in its large (60S) subunit (Barakat et al., 2001). In plants, rRNAs are encoded by 5S and 45S rDNA genes, which are transcribed in the nucleoplasm and the nucleolus by RNA polymerase III or RNA polymerase I, respectively. All eukaryotic genomes include hundreds of rDNA genes arranged in tandem in several loci. Each 45S rDNA gene is composed (from its 5′ to 3′ end) of a promoter and a transcriptional unit that contains the 5′ external transcribed spacer (5′-ETS), the 18S, 5.8S and 25S rRNA sequences (in plants and yeast; 28S in animals), and a 3′-ETS. These three regions encoding rRNAs are separated by two internal transcribed spacers: ITS1 is located between the sequences of the 18S and 5.8S rRNAs, while ITS2 is located between the sequences of the 5.8S and 28S/25S rRNAs (Supplemental Figure 1).

The processing of 45S (47S in animals and 35S in yeast [*Saccharomyces cerevisiae*]) pre-rRNA is a multistep procedure involving more than 100 ribosome biogenesis factors (RBFs), which carry out endo- and exo-nucleolytic cleavages and chemical modifications to generate 28S/25S, 18S and 5.8S mature rRNAs. This intricate rRNA production consists of two partially redundant pathways, which are named according to the region of the early 35S(P) pre-rRNA in which the first endonucleolytic cleavage occurs: the 5′-ETS-first and ITS1-first pathways. There is an additional pathway in plants, the ITS2-first pathway (Supplemental Figure 1; Palm et al., 2019). The functions of many RBFs are partially or fully conserved across animals, fungi and plants (reviewed in Sáez-Vásquez and Delseny, 2019).

Yeast mRNA transport4 (Mtr4) is an ATP-dependent RNA helicase that acts as a cofactor of the nucleolar exosome, which has 3′→5′ exonuclease activity. Loss-of-function mutations of the yeast *Mtr4* gene impairs 5.8S and 25S rRNA maturation through the ITS1-first pathway and leads to an imbalance in the ratio of 40S/60S ribosomal subunits (Thoms et al., 2015). Arabidopsis MTR4 is required for 18S and 5.8S rRNA maturation and to eliminate 5′-ETS processing by-products produced in the ITS1-first pathway (Lange et al., 2011). Yeast Mtr4 interacts with Nucleolar protein 53 (Nop53), which has orthologs in humans (Glioma Tumor-Suppressor Candidate Region 2; GLTSCR2) and Arabidopsis (SMALL ORGAN 4; SMO4), all of which are involved in equivalent steps of 5.8S rRNA maturation (Tafforeau et al., 2013; Micol-Ponce et al., 2020). Ribosomal RNA processing protein 7 (Rrp7) is another yeast RBF involved in 18S rRNA processing that functions in the ITS1-first pathway, as do its human

(RRP7A) and Arabidopsis (RRP7) orthologs (Micol-Ponce et al., 2018; Farooq et al., 2020; Supplemental Figure 1).

Most RPs that form part of the 40S ribosomal subunit also function as RBFs in the nuclear and cytoplasmic steps of 18S rRNA maturation in yeast, including Ribosomal protein S24 (Rps24; Ferreira-Cerca et al., 2005). Human RPS24 and yeast Rps24 play analogous roles in 5′-ETS processing. Loss-of-function mutations of the yeast *Rps24* and human *RPS24* orthologs lead to the accumulation of 23S and 30S pre-rRNAs, respectively (which are equivalent to Arabidopsis P-A_3 pre-rRNA) and a reduction in the amounts of human 21S and 18S-E, and yeast 21S and 20S pre-rRNAs, which are equivalent to Arabidopsis 18S-A_3 and 20S, respectively. All of these pre-rRNAs are precursors of the 18S rRNA produced by the ITS1-first pathway (Supplemental Figure 1). Since this pathway is the major contributor to 18S rRNA production, its level is reduced by human and yeast *rps24* loss-of-function mutations (Ferreira-Cerca et al., 2005; Choesmel et al., 2008).

Arabidopsis *MORPHOLOGY OF ARGONAUTE1-52 SUPPRESSED 2* (*MAS2*) is the ortholog of the human gene encoding NF-κ-B-activating protein (NKAP), which functions in transcriptional repression and splicing in animals (Pajerowski et al., 2009; Burgute et al., 2014; Sánchez-García et al., 2015). We previously identified physical interactors of MAS2 in a yeast two-hybrid assay (Sánchez-García et al., 2015), including RRP7 (Micol-Ponce et al., 2018), SMO4 (Micol-Ponce et al., 2020) and RPS24B. Here, we studied the functions of the Arabidopsis co-orthologs of yeast *Rps24* and human *RPS24*: AT3G04920 and AT5G28060, which encode RPS24A and RPS24B, respectively. We established that both RPS24A and RPS24B act as RBFs in the ITS1-first pathway, like their human and yeast orthologs. Our results also suggest that RPS24A and RPS24B participate in the transcriptional repression of 45S rDNA, a role that has not been proposed for any of their orthologs.

RESULTS

Arabidopsis *RPS24A* and *RPS24B* show combined haploinsufficiency

The Arabidopsis *RPS24A* (AT3G04920) and *RPS24B* (AT5G28060) genes are very similar in structure, with 5 exons, and their protein products sharing 96% sequence identity (Supplemental Figure 2). We initially focused our study on RPS24B, since we previously showed that it interacted with MAS2 in a Y2H assay (Sánchez-García et al., 2015). Two putatively null alleles of *RPS24B*, *rps24b-1* and *rps24b-2*, were previously identified as mutants with impaired leaf development; *rps24b-1* harbors a 72-bp deletion in the coding region of its fifth exon (Horiguchi et al., 2006; 2011), and *rps24b-2* carries a T-DNA insertion in its third intron (Figure 1A; Horiguchi et al., 2011; Wang et al., 2018). Both mutants exhibited an almost identical mild pointed-leaf phenotype (Figure 1F; Horiguchi et al., 2011; Wang et al., 2018).

The *apiculata6* (*api6*) mutant was previously isolated in a large-scale screen for leaf morphological mutants from an EMS mutagenized population in the L*er* background (Berná et al., 1999). Using iterative linkage analysis (Ponce et al., 1999; Ponce et al., 2006), we mapped the *api6* mutation to a genomic region containing 49 genes flanked by the molecular markers cer449133 (between AT5G27905 and AT5G27910) and cer451402 (in AT5G28200; Supplemental Table 1). Sanger sequencing of AT5G28060 (*RPS24B*), the most plausible candidate gene, revealed an EMS-type G→A transition in the last nucleotide of the first intron (Figure 1A). Since this nucleotide forms part of a 3′ splicing site (3′SS) of the first intron, the *api6* mutation is predicted to cause the absence of the second exon of the gene—which is 42-nt in length—from the mature mRNA of *api6* (Figure 1B and C). The protein produced by the *api6* mutant is predicted to lack 14 residues present in wild-type RPS24B (amino acids 25-38; Supplemental Figure 2). An *api6* × *rps24b-2* cross confirmed that these mutants are allelic (Figure 1E, F, H-J). Like many mutants in the L*er* genetic background, the leaf phenotype of *api6* was stronger than that of *rps24b-1* or *rps24b-2*, which are in the Col-0 background (Pérez-Pérez et al., 2009).

We also studied SALK_126799, a line that carries a T-DNA insertion in the third intron of *RPS24A,* which we named *rps24a-1* (Figure 1D and G). Homozygous *rps24a-1* plants were viable and exhibited a pointed-leaf phenotype, which was milder than that of *rps24b-2* and *api6* (Figure 1E-I). RPS24A and RPS24B exhibited similar protein abundance patterns, as determined in the Arabidopsis THaliana ExpressioN Atlas (Athena) database (http://athena.proteomics.wzw.tum.de:5002/master_arabidopsisshiny/; Mergner et al., 2020), with similar levels throughout all organs and developmental stages, with a few exceptions (Supplemental Dataset 1 [highlighted in red]). The almost constitutive

expression of *RPS24A* and *RPS24B* (at a lower level compared to other genes encoding RPs) was also described by Savada and Bonham-Smith (2014) using microarray data from the GENEVESTIGATOR platform (Hruz et al., 2008).

Since the mutant phenotypes of *rps24a-1* and *rps24b-2* pointed to the functional redundancy of *RPS24A* and *RPS24B*, we performed *rps24a-1* × *rps24b-2* reciprocal crosses. All *RPS24A/rps24a-1;RPS24B/rps24b-2* F_1 plants exhibited a mutant phenotype indistinguishable from that of their parents, suggesting non-allelic non-complementation (Figure 2A-D). Selfing of such diheterozygotes generated F_2 progeny with only two phenotypic classes: 221 wild-type and 161 mutant (indistinguishable from their parents) plants. We genotyped 59 F_2 phenotypically mutant plants, finding 10 *rps24a-1/rps24a-1 RPS24B/RPS24B*, 17 *RPS24A/RPS24A rps24b-2/rps24b-2* and 32 *RPS24A/rps24a-1;RPS24B/rps24b-2* plants. We identified no *rps24a-1/rps24a-1;RPS24B/rps24b-2* or *RPS24A/rps24a-1;rps24b-2/rps24b-2* sesquimutants or double mutants among the F_2 progeny (Figure 2A-D); the absence of these genotypes suggests their conditional lethality. In agreement with the proposed early lethality of the genotypes with fewer than two wild-type doses of either *RPS24A* or *RPS24B* (expected to be 31.25% of seeds), the siliques of several diheterozygous F_1 plants exhibited a rate of 27% aborted or unfertilized ovules compared to Col-0 (Figure 2E-H).

To determine whether *rps24a-1*, *rps24b-2* and *api6* were hypomorphic or null mutants and to test the existence of any dosage compensation mechanism for the expression of *RPS24A* or *RPS24B*, we analyzed *RPS24B* mRNA levels by RT-PCR. We used primers upstream and downstream of the T-DNA insertion of *rps24b-2* (Supplemental Figure 3 and Supplemental Table 2). *RPS24B* mRNA levels were very similar in *api6* and L*er*, but *RPS24B* mRNA levels were undetectable in *rps24b-2* and were not higher in *rps24a-1* than in the wild type (Supplemental Figure 3). We did not determine whether *rps24a-1* was null, because it was impossible to design RT-PCR primers specific for this allele that would amplify the region flanking its T-DNA insertion, due to its sequence similarity with *rps24b-2*. However, the phenotype of the single mutants and the lethality of the reciprocal sesquimutants strongly suggest that *rps24a-1* and *rps24b-2* are null alleles.

RPS24B predominantly localizes to the nucleolus

Since ribosomal subunits are synthetized and assembled in the nucleolus and the nucleoplasm, but their final maturation occurs in the cytoplasm, not few RPs have been detected in all three subcellular compartments (Pendle et al., 2005; Palm et al., 2016; Montacié et al., 2017; Ayash et al., 2021). As expected from their known roles as structural components of the ribosome, Arabidopsis RPS24A and RPS24B have been

found in the cytoplasm in several proteomic studies (Chang et al., 2005; Giavalisco et al., 2005; Carroll et al., 2008; Hummel et al., 2015), and their abundances appear to be similar, at least in ribosomes purified from cell cultures (Salih et al., 2020). RPS24A and RPS24B have also been localized to the nucleolus and nucleoplasm (Pendle et al., 2005; Palm et al., 2016; Montacié et al., 2017; Ayash et al., 2021).

To visualize the subcellular localization of RPS24B, we generated the *35S$_{pro}$:RPS24B:GFP* construct and used it to transform Col-0 plants. We primarily detected green fluorescent protein (GFP) fluorescence in the nucleolus, but also in the cytoplasm (Figure 3), as observed for other duplicated Arabidopsis RPs of the small and large subunits: RPS3aA/B, RPS8A/B, RPL7aA/B, RPL15A/B and RPL23aA/B (Savada and Bonham-Smith, 2014). Three protein-localization predictor tools provided in silico support to our experimental findings with the *35S$_{pro}$:RPS24B:GFP* transgenic plants. LOCALIZER (https://localizer.csiro.au/; Sperschneider et al., 2017) identified a putative nuclear localization signal (NLS) in the C-terminal regions of RPS24A and RPS24B, which matches the nucleolar localization signal (NoLS) found using Nucleolar localization sequence Detector (NoD) software (Supplemental Figure 2; http://www.compbio.dundee.ac.uk/www-nod/index.jsp; Scott et al., 2011). MULocDeep (https://www.mu-loc.org; Jiang et al., 2021), which is able to predict the localization of any protein in 44 suborganellar compartments, clearly predicted a nucleolar localization for both RPS24 proteins, in addition to a lower-likelihood prediction for a cytoplasmic and mitochondrial localization (Supplemental Figures 4 and 5). The predicted nucleolar localization of RPS24A and experimental confirmation for RPS24B suggest that both proteins function in early steps of ribosome biogenesis. However, although the subcellular localization of the RPS24B-GFP fusion protein was the same in transgenic plants in the Col-0 or *rps24b*-2 background, the *35S$_{pro}$:RPS24B:GFP* transgene did not rescue the morphological defects caused by the *rps24b-2* mutation.

45S pre-rRNA processing is delayed in the *rps24* mutants

As previously mentioned, human and yeast RPS24 act as RBFs in 18S rRNA maturation. In both species, depletion of RPS24 results in inhibited 5′-ETS processing, the accumulation of pre-rRNAs that include 5′-ETS (human 30S and yeast 23S pre-rRNAs) and reduced levels of 21S and 18S-E pre-rRNAs in humans and their corresponding 21S and 20S pre-RNAs in yeast (Supplemental Figure 1), all of which are 18S rRNA precursors (Ferreira-Cerca et al., 2005; Choesmel et al., 2008; Robledo et al., 2008).

Taken together, the current identification of RPS24B as a predominantly nucleolar factor and the previous finding of RPS24A and RPS24B in the Arabidopsis

nucleolar proteome via large-scale analysis (Pendle et al., 2005; Palm et al., 2016) point to a conserved role for these proteins as RBFs. To test this hypothesis, we analyzed 45S pre-rRNA processing in the *rps24* mutants. We carried out gel blot analysis of total RNA extracted from *rps24a-1*, *rps24b-2* and *api6*, which was hybridized with the S2, S7 and S9 probes. These probes are complementary to segments of the 5′-ETS, ITS1, and ITS2 of 45S pre-rRNA, respectively, allowing several 25S, 18S and 5.8S rRNA precursors to be detected (Figure 4A). We used the *smo4-3* and *mtr4-2* mutants as controls (Lange et al., 2011; Micol-Ponce et al., 2020). Loss of SMO4 function causes nucleolar hypertrophy and the accumulation of P-A_3, a precursor of 18S rRNA, and perturbs 5.8S rRNA maturation (Micol-Ponce et al., 2020). MTR4 is an exosome cofactor involved in the processing of 5.8S pre-rRNA (like SMO4) but also in the degradation of P-P′, a by-product derived from 5′-ETS processing (Lange et al., 2011).

Using the S7 probe, we detected the accumulation of P-A_3 and $35S_{A123B}$/35S(P) pre-rRNAs in *rps24a-1*, *rps24b-2* and (especially) *api6* plants compared to their respective wild types. We also detected the depletion of 33S(P′)/32S pre-rRNA and to a lesser extent P′-A_3/18S-A_3/18S-A_2 species, which result from the processing of $35S_{A123B}$/35S(P) and P-A_3 precursors, respectively (Figure 4B). P-A_3 pre-rRNA is generated by the cleavage of the A_3 site in 35S(P) pre-rRNA, the first 18S rRNA precursor in the ITS1-first pathway [Figure 4A and Supplemental Figure 1; reviewed in Sáez-Vásquez and Delseny (2019)]. We confirmed the accumulation of $35S_{A123B}$/35S(P) and P-A_3 pre-rRNAs using the S2 probe, but we only observed the accumulation of the P-P′ species in *mtr4-2* (Figure 4C), as previously described (Lange et al., 2011). Using the S9 probe, we did not find any alteration in 5.8S rRNA maturation in any of the three mutants studied (Figure 4D).

Reduced levels of the 21S and 18S-E precursors of 18S pre-rRNA (Supplemental Figure 1) associated with the lack of RPS24 activity in human cells result in a 40% reduction in mature 18S rRNA levels (Choesmel et al., 2008; Robledo et al., 2008). Similar effects were found in the absence of RPS24 function in yeast: 35S, 32S and 23S pre-rRNAs accumulated, 20S pre-rRNA could not be detected, and the levels of mature 18S rRNA were reduced by 95% compared to the wild type (Ferreira-Cerca et al., 2005). The impaired 18S pre-rRNA processing due to the loss of RPS24A and RPS24B function in Arabidopsis suggests that the levels of mature 18S rRNA might be reduced in these mutants. Therefore, we analyzed the rRNA profiles of the mutants using a bioanalyzer. The 18S/25S rRNA ratio was reduced by 4% in the *rps24a-1* mutant, by 27% in *rps24b-2* and by 32% in *api6* compared to their corresponding wild types (Supplemental Figure 6). These results provide further

evidence for a conserved role for RPS24A and RPS24B in the early steps of 18S rRNA maturation, particularly in the cleavage of sites internal to the 5′-ETS, as already observed for their yeast and human putative orthologs (Ferreira-Cerca et al., 2005; Choesmel et al., 2008).

The *rps24b-2* mutation enhances the morphological and molecular defects of mutants in genes encoding RBFs that function in 18S and 5.8S rRNA maturation

To genetically confirm the involvement of RPS24 in ribosome biogenesis, we obtained double mutant combinations between *rps24b-2* and mutant alleles of *SMO4* and *MTR4*, which participate in 5.8S rRNA maturation (Lange et al., 2011; Micol-Ponce et al., 2020) and *RRP7* and *PARALLEL1* (*PARL1*; also named *NUCLEOLIN1*), which act in 18S rRNA maturation (Pontvianne et al., 2007; Micol-Ponce et al., 2018).

All of the double mutants showed synergistic phenotypes (Figure 5). Leaves of *rps24b*-2 *smo4-2* plants exhibited increased serration and took on a twisted appearance into a spiral (Figure 5F). *rps24b*-2 *mtr4-2* plants exhibited delayed growth, lanceolate leaves and strong drops in rosette size and plant height (Figure 5G). *rps24b-2 parl1-2* plants strongly accumulated anthocyanins, exhibiting dark, serrated, pointed leaves and small, compact rosettes (Figure 5H). The *rps24b-2 mtr4-2* and *rps24b-2 parl1-2* double mutants completed their lifecycles but had poor fertility (Figure 5I, J, M-P). We sowed 108 F_2 seeds from an *rps24b-2* × *rrp7-1* cross and isolated two double mutants, which exhibited very strong mutant phenotypes (Supplemental Figure 7). Only one plant completed its lifecycle and produced 20 F_3 seeds, only one of which germinated, but the seedling died a few days later, suggesting early postembryonic lethality of the *rps24b-2 rrp7-1* genotype.

We analyzed 45S pre-rRNA maturation in the viable double mutants, finding similar levels of P-A_3 or P′-A_3/18S-A_3/18S-A_2 pre-rRNAs in *rps24b-2 smo4-3*, *rps24b-2 mtr4-2* and *rps24b-2 parl1-2* compared to the single mutants using the S2 and S7 probes (Figure 6A and B). The *smo4-3* and *mtr4-2* single mutants accumulate 7S and 5.8S+10 pre-rRNAs, respectively (Lange et al., 2011; Micol-Ponce et al., 2020). Unexpectedly, using the S9 probe, we detected higher levels of 7S pre-rRNA in *rps24b*-2 *smo4-3* and of 5.8S+10 pre-rRNA in *rps24b-2 mtr4-2* compared to the *smo4-3* and *mtr4-2* single mutants, even though *rps24b-2* did not accumulate either of these pre-rRNA species (Figure 6C and D).

To assess the subcellular localization of 5.8S pre-rRNA in the *rps24b*-2 *smo4-3* and *rps24b*-2 *mtr4-2* double mutants, we performed an RNA-FISH assay. We used the 23-nt long S9 probe, which hybridizes to the ITS2 region adjacent to the 5.8S rRNA coding sequence, and allows detection of all 5.8S pre-rRNA, but not mature 5.8S rRNA

(Figure 4A). In agreement with the results of RNA gel blot analysis (Figure 6C and D), we observed very low fluorescence in the nucleoli of wild-type Col-0 and L*er*, higher fluorescence in the *api6*, *rps24a-1*, *rps24b-2*, *smo4-3* and *mtr4-2* single mutants, and much higher fluorescence in the *rps24b*-2 *smo4-3* and *rps24b*-2 *mtr4-2* double mutants (Supplemental Figure 8). The enhanced fluorescence that we observed in the nucleoli of *rps24* mutants compared to Col-0 and L*er* is likely due to the accumulation of the $35S_{A123B}$/35S(P) species that we detected in RNA gel blots using the S7 and S9 probes (Figure 4B-D).

In the RNA-FISH assays, we also observed enlarged nucleoli in *rps24b-2* and (especially) *smo4-3 rps24b-2* and *mtr4-2 rps24b-2* double mutant plants compared to Col-0 (Supplemental Figure 8). Perturbations in the size and organization of the nucleolus are hallmarks of nucleolar stress, which occurs when ribosome biogenesis is defective, as previously observed in the nucleoli of *smo4* plants (Micol-Ponce et al., 2020). Therefore, we measured the areas of the nucleolus and nucleoplasm using the fluorescence of the S9 probe and of nuclei stained with DAPI. Both the nucleus and nucleolus of *api6* and *rps24b-2* (but not *rps24a-1*) were larger than those of the respective wild types (Supplemental Figure 8A2 and A3). Moreover, the nucleus and nucleolus were greatly enlarged in both the *smo4-3 rps24b-2* and *mtr4-2 rps24b-2* double mutants (Supplemental Figure 8D-F, J-L, P-R, V-A3).

To determine whether the organization of the nucleolus was perturbed in the *rps24* mutants, we used an antibody against the nucleolar marker fibrillarin to examine the roots of Col-0, *rps24a-1* and *rps24b-2* seedlings. We did not observe differences in nucleolar organization between the wild type and mutants (Supplemental Figure 9), suggesting that the defective 45S pre-rRNA processing in the *rps24* mutants causes the enlargement but not disorganization of the nucleolus.

Taken together, these results suggest that RPS24B participates (directly or indirectly) in the maturation of 5.8S rRNA. Since the *rps24a-1* and *rps24b-2* single mutants do not accumulate any 5.8S pre-rRNA, RPS24B might play a lesser role in 5.8S maturation compared to SMO4 and MTR4; therefore, the absence of RPS24B is only perceived in the absence of SMO4 and MTR4. Another interpretation is that RPS24 participates in the repression of 45S rDNA transcription. Under this second scenario, the accumulation of 5.8S pre-rRNAs would be more evident in the *rps24b* background than in the *smo4-3* and *mtr4-2* single mutant backgrounds due to the presence of more 5.8S pre-rRNAs to process.

45S pre-rRNAs accumulate in the *rps24* mutants

325 Kinetic analysis of Arabidopsis 45S pre-rRNA processing has revealed three rate-
326 limiting steps: the processing of 35S, 32S, and P-A_3 pre-rRNAs; 32S and P-A_3 pre-
327 rRNAs are the first two precursors in the two alternative pathways, the 5'-ETS first
328 pathway and the ITS1-first pathway, respectively (Supplemental Figure 1). The level of
329 35S pre-rRNA is the major indicator of the transcription rate of 45S rDNA (Shanmugam
330 et al., 2021). Our results show that a reduction in RPS24 activity lower the rate of 45S
331 pre-rRNA processing, as shown by the accumulation of pre-rRNAs produced by two of
332 the rate-limiting steps, $35S_{A123B}$/35S(P) and P-A_3. Our results also suggest that 45S
333 rDNA transcription is upregulated in the *rps24* mutants.
334 Therefore, we performed RT-PCR to investigate the presence of the four
335 different 45S rDNA variants (*VAR*s), which differ in their 3′-ETS (Figure 8A), using the
336 p3+p4 primer pair (Figure 7A and B; Supplemental Table 2). We did not detect any
337 differences in the intensities of the PCR bands using genomic DNA as a template
338 (Figure 7C). However, the intensities of the PCR bands corresponding to *VAR4*, *VAR2*
339 and *VAR3* were higher in *rps24a-1*, and those corresponding to all four *VARs* were
340 higher in *rps24b-2*, compared to the wild type (Figure 7D). Since changes in the
341 relative abundance of 45S rRNA variants are usually interpreted as changes in 45S
342 rDNA transcription (Kojima et al., 2007; Pontvianne et al., 2010; Durut et al., 2014),
343 these results suggest that RPS24B represses 45S rDNA expression.
344 To confirm these results, we carried out RT-qPCR analysis using the 45S pre-
345 rRNA-45S-F and 45S pre-rRNA-45S-R primers, which hybridize to the 5′-ETS
346 (Supplemental Table 2; Zhu et al., 2016). We detected higher levels of 45S pre-rRNA
347 in the *rps24* mutants than in wild-type plants (Figure 7E).
348
349 **RPS24B-GFP co-precipitates with nucleolar factors involved in ribosome**
350 **biogenesis and pre-mRNA splicing**
351 To identify nucleolar interactors of RPS24B, we carried out co-immunoprecipitation
352 (Co-IP) assays with an anti-GFP antibody in Col-0 plants harboring the
353 *$35S_{pro}$:RPS24B:GFP* transgene. The raw list of 2,635 proteins that co-purified with
354 RPS24B-GFP was filtered by considering only those classified as high-confidence
355 proteins (q-value <0.01) with at least two peptide spectra matches (PSMs) in each of
356 the three biological replicates (Supplemental Dataset 2). Several additional filters were
357 used, which discarded proteins that co-immunoprecipitated with all four other proteins
358 examined (none related to ribosome biogenesis), as we considered these to be
359 spurious interactions. We analyzed the predicted suborganellar localizations of the
360 interactors using MuLOCDeep (Jiang et al., 2021), discarding those that were not
361 predicted to be nucleolar proteins, which reduced the list of putative interactors to 25

362 proteins (Supplemental Dataset 2). We refined the annotations of these proteins using
363 the TAIR or Aramemnon database and those identified in two independent nucleolar
364 proteomic analyses (Palm et al., 2016; Montacié et al., 2017). In addition, we added the
365 pathways that were enriched in genes that were co-expressed with the genes encoding
366 the 25 putative interactors of RPS24B obtained from the ATTEDII database (Obayashi
367 et al., 2022).

368 We found ten proteins encoded by genes whose co-expression was enriched in
369 ribosome components, which included six RPs, six whose co-expression was enriched
370 in genes involved in ribosome biogenesis, three in spliceosome components, and two
371 in RNA transport, but that were components of the spliceosome: PRE-MRNA
372 PROCESSING FACTOR 8 (PRP8), the main component of the spliceosome, and one
373 of its major interactors during pre-mRNA splicing, the putative RNA helicase BAD
374 RESPONSE TO REFRIGERATION2 (BRR2; Nguyen et al., 2013).

375 Among the putative interactors identified by co-immunoprecipitation that were
376 encoded by genes that are co-expressed with genes involved in ribosome biogenesis,
377 we found AT3G05060 (*NOP58-2*) and AT5G27120 (*NOP58-1*); these genes encode
378 the co-orthologs of *NOP58* in yeast and humans, which are putative components of the
379 C/D small nucleolar ribonucleoprotein (snoRNP) complex. AT1G31970 and
380 AT1G77030, encoding DEA(D/H)-box RNA helicases, were two other co-expressed
381 genes that are putative orthologs of yeast *DEAD-box protein 3* (*DBP3*) and *DBP10*,
382 respectively, both of which are involved in 60S subunit biogenesis. DBP3 functions in
383 the endonucleolytic cleavage of site A_3 in ITS1, upstream of 5.8S rRNA (Weaver et al.,
384 1997), and DBP10 functions in the cleavage of sites C_1 and C_2 in the ITS2 (Burger et
385 al., 2000). AT1G31970 encodes STRESS RESPONSE SUPPRESSOR 1 (STRS1), a
386 nucleolar- and chromocenter-localized protein that undergo stress-mediated
387 relocalization and is involved in epigenetic gene silencing at heterochromatic loci; its
388 mutants show reduced DNA methylation at these loci (Khan et al., 2014). AT1G77030
389 encodes the putative DEAD-box ATP-dependent RNA HELICASE 29 (RH29), which
390 has not been studied in Arabidopsis. AT3G56510, AT5G04600 and AT5G57120 have
391 not been studied either. AT3G56510 is annotated at the Aramemnon database
392 (Schwacke et al., 2003) as the putative ortholog of yeast Eighteen S rRNA Factor 2
393 (Esf2), a nucleolar component of the small subunit processome (SSU) involved in early
394 steps of 18S rRNA maturation. Yeast Esf2 associates with 5′-ETS and is required for
395 SSU assembly and compaction. The *esf2* mutants show defective cleavage of sites A0
396 (within the 5′-ETS) through A2 (within the ITS1), therefore exhibiting reduced 18S rRNA
397 production (Hoang et al., 2005). AT5G04600 encodes the putative ortholog of human
398 NUCLEOLAR PROTEIN INTERACTING WITH THE FHA DOMAIN OF MKI67 (NIFK),

399 an RBF involved in endonucleolytic ITS2 cleavage that is required for 28S and 5.8S
400 rRNA maturation (Pan et al., 2015). Finally, AT5G57120 encodes the putative ortholog
401 of yeast serine rich protein 40 (SRP40) and human nucleolar and coiled-body
402 phosphoprotein 1 (NOLC1), also named Nopp140 (140 kDa nucleolar phosphoprotein),
403 which might function as chaperones of snoRNP complexes (Yang et al., 2000).

404 **DISCUSSION**

405 **The Arabidopsis *RPS24A* and *RPS24B* paralogs exhibit combined**
406 **haploinsufficiency**

407 The ribosome has traditionally been considered to be a highly conserved housekeeping
408 machinery, as it is present in all cells of all organisms. In prokaryotic and eukaryotic
409 ribosomes, the number of RPs is almost identical, i.e., 55 and 79, respectively.
410 However, proteomic analyses of animals, plants and fungi have revealed the existence
411 of different ribosomes with heterogeneous compositions and stoichiometry, suggesting
412 that specialized ribosomes might translate different sets of mRNAs. Such heterogeneity
413 in composition results from the existence of different paralogous genes produced by
414 gene duplications. These genes, with similar architectures and variable numbers
415 among species, encode quasi-identical RPs [reviewed in Martinez-Seidel et al. (2020;
416 Petibon et al. (2021)].

417 Plants have undergone more frequent gene and genomic duplications during
418 evolution compared to metazoans, leading to families of RPs with two to seven
419 paralogs in Arabidopsis (Carroll et al., 2008). In Arabidopsis, the RPs of the
420 cytoplasmic ribosome appear to be encoded by 234 functional genes, whereas the
421 ribosomes of humans and yeast include proteins encoded by 85 and 137 genes,
422 respectively (Barakat et al., 2001; Chang et al., 2005; Carroll et al., 2008). In the quasi-
423 identical RP pairs studied to date, one of the two paralogous genes is sometimes
424 expressed at a higher level and contributes more to ribosome structure than the other
425 gene. In other cases, their levels of expression and contributions to the ribosome are
426 equivalent [reviewed in Petibon et al. (2021)]. Loss of function of either gene of a pair
427 produces a similar mutant phenotype, indicating that both paralogs are required for
428 normal development (Savada and Bonham-Smith, 2014; Salih et al., 2020; Xiong et al.,
429 2021).

430 Haploinsufficiency describes the requirement for more than one wild-type allele
431 for normal development or viability for single-copy genes. Combined haploinsufficiency
432 describes a situation in which two paralogous genes behave as a single
433 haploinsufficient unit with four alleles. *RPS24A* and *RPS24B* provide such an example
434 of combined haploinsufficiency, since three wild-type doses of *RPS24* are required for
435 proper plant development and two for viability. It is worth noting that the single-copy
436 human *RPS24* gene is a haploinsufficient locus. Haploinsufficiency is observed in
437 several human genetic diseases, such as Diamond-Blackfan anemia (DBA), a
438 ribosomopathy (Gazda et al., 2006) associated with the loss-of-function of *RPS24*, as
439 well as other genes encoding RPs (Tyagi et al., 2020). Ribosomopathies are diseases

440 caused by mutations in genes encoding components of the ribosome, with tissue-
441 specific effects and an increased risk of cancer [reviewed in Kang et al. (2021)].
442 *RPS24A* and *RPS24B* have similar expression patterns and contributions to the
443 composition of Arabidopsis ribosomes, pointing to their functional equivalence and
444 partial redundancy. However, the mRNA levels of *RPS24A* and *RPS24B* are lower than
445 those of other genes encoding RPs (Savada and Bonham-Smith, 2014). Here we
446 demonstrated that these genes do not show dosage compensation; i.e., *RPS24A* is not
447 more expressed in the absence of *RPS24B*. A proper stoichiometry of ribosome
448 structural components is crucial for ribosome function (Warner, 1999; Slavov et al.,
449 2015; Ni and Buszczak, 2023), and our results suggest that the amount of RPS24A
450 and RPS24B produced in Arabidopsis cells is limiting for ribosome production. Indeed,
451 reduction in the wild-type doses of either protein in *rps24a* and *rps24b* single mutants
452 and diheterozygous plants (Figures 1 and 2) decreases the number of productive
453 ribosomes, resulting in an inadequate rate of protein synthesis. This phenomenon of
454 non-allelic non-complementation is also observed in mutants affected in other
455 Arabidopsis genes encoding RPs, including *RPS6*, *RPL5*, *RPL23* and *RPL36*
456 (Degenhardt and Bonham-Smith, 2008; Fujikura et al., 2009; Creff et al., 2010;
457 Casanova-Sáez et al., 2014).
458
459 **RPS24A and RPS24B function as RBFs during 18S rRNA maturation, like their**
460 **yeast and human orthologs**
461 Gene duplications have allowed some RPs to acquire additional functions that might or
462 might not be related to translation. In Arabidopsis, besides their functions as structural
463 proteins of the ribosome, only RPS2 was shown to function as an RBF during the
464 maturation of 25S and 18S rRNA and RPS6 in the transcriptional regulation of 45S
465 rDNA (Kim et al., 2014; Hang et al., 2021). PROTEIN ARGININE
466 METHYLTRANSFERASE 3 (PRMT3) and RPS2B (one of the six paralogs encoded in
467 the Arabidopsis genome) facilitate the assembly and disassembly of the SSU
468 processome (or 90S) and repress nucleolar stress (Hang et al., 2021). RPS6, encoded
469 by two functionally equivalent paralogs, interacts with HISTONE DEACETYLASE 2
470 (HDA2) in the nucleus and nucleolus and binds to the promoter of 45S rDNA,
471 controlling its transcription (Kim et al., 2014). Furthermore, RPL10 is related to
472 responses to ultraviolet light stress and viral infection, and RPL24 is involved in
473 microRNA biogenesis (Carvalho et al., 2008; Ferreyra et al., 2010a; Ferreyra et al.,
474 2010b; Li et al., 2017).
475 Our results show that both Arabidopsis RPS24A and RPS24B function as RBFs
476 in the early steps of 45S pre-rRNA processing, specifically at the P′ site of the 5′-ETS.

In the *rps24b-2*, *api6* and *rps24a-1* mutants, we detected the accumulation of $35S_{A123B}$/35S(P) pre-rRNA (the first intermediate in 45S pre-rRNA processing) and a reduction in the levels of 33S(P′)/32S species (the second intermediates in this processing; Supplemental Figure 1). We also detected defects in the processing of 18S pre-rRNA: the *rps24b-2*, *api6* and *rps24a-1* mutants accumulated P-A_3 pre-rRNA and showed reduced levels of P′-A_3/18S-A_3/18S-A_2 pre-rRNAs (Figure 4). These results suggest that the loss-of-function of *RPS24A* and *RPS24B* globally reduces the processing of 5′-ETS, as occurs in response to the loss-of-function of yeast and human *RPS24* (Ferreira-Cerca et al., 2005; Choesmel et al., 2008; Robledo et al., 2008). Moreover, the *rps24b* mutant showed an imbalance in the 25S/18S ratio, suggesting that alterations in the processing of pre-rRNAs of the ITS1-first pathway lead to a decrease in 18S rRNA levels.

RPS24B* genetically interacts with *NOP53* (*SMO4*) and *MTR4

We obtained double mutant combinations of *rps24b-2* with mutant alleles of genes involved in different steps of 45S pre-rRNA processing. Two such double mutants exhibited synergistic phenotypes: *rps24b-2 rrp7-1* was embryonic lethal, and *rps24b-2 mtr4-2* had a dwarf stature, with poor fertility. The phenotypes of *rps24b-2 smo4-3* were also synergistic, as this mutant was also nearly fully sterile (Figure 5).

We previously demonstrated that RRP7 is involved in 18S rRNA maturation and acts as a repressor of 45S rDNA transcription. The *rrp7* mutant has a reduced 18S/25S rRNA ratio and accumulated P-A_3 pre-rRNA (Micol-Ponce et al., 2018), similar to findings for the *rps24* mutant. Moreover, we reasoned that RRP7 might function as a repressor of 45S rDNA, as *rrp7* showed heterochronic expression of *VAR1* and increased *VAR3* expression (Micol-Ponce et al., 2018). Here, we determined that *rps24a-1* and *rps24b-2* contained increased levels of 45S pre-rRNA (Figure 7), which might explain the synergistic phenotype of the *rps24b-2 rrp7-1* double mutant. However, due to the lethality of *rps24b-2 rrp7-1*, we were unable to examine the effects of the combination of both mutations on the maturation of 18S rRNA and/or the transcription of 45S rDNA.

NOP53 (SMO4 in Arabidopsis) and MTR4 are RBFs that function in the maturation of 5.8S rRNA (Lange et al., 2011; Micol-Ponce et al., 2020). MTR4 is a cofactor of the exosome, which also functions in the degradation of P-P′, the by-product of 5′-ETS (Lange et al., 2011). Loss-of-function of *SMO4* or *MTR4* leads to the accumulation of 7S or 5.8S + 70-nt pre-rRNAs, respectively (which are precursors of 5.8S rRNA that are processed in the nucleolus) but not 6S rRNA (the final precursor of 5.8S rRNA maturation that is processed after its export to the cytoplasm; Lange et al.,

514 2011; Micol-Ponce et al., 2020). In the current study, we did not detect the
515 accumulation of P-P′ or any 5.8S pre-rRNA in the *rps24a* or *rps24b* mutant, suggesting
516 that RPS24A and RPS24B do not participate in these steps of 45S pre-rRNA
517 processing. However, we unexpectedly detected the over-accumulation of specific 5.8S
518 pre-rRNAs in *smo4-3* and *mtr4-2* and in the double mutants *rps24b-2 smo4-3* and
519 *rps24b-2 mtr4-2* (Figure 6). Such over-accumulation may explain their synergistic
520 phenotypic defects of these mutants. Our RNA-FISH analysis with the S9 probe
521 confirmed these results, revealing strong fluorescent signals in the nucleoli of the
522 double mutants (Supplemental Figure 8).

523 One possible explanation of these results is that RPS24B (and possibly
524 RPS24A) functions in 5.8S rRNA maturation, albeit to a lesser extent than SMO4 and
525 MTR4. An alternative hypothesis is that the over-accumulation of 7S and 5.8S + 70-nt
526 pre-rRNAs, which we detected in *rps24b-2 mtr4-2* and *rps24b-2 smo4*-3 plants,
527 respectively, is due to an increase in rDNA transcription caused by the *rps24b-2*
528 mutation. If more pre-rRNAs are available for processing, the steps involving MTR4
529 and SMO4 are likely to be more strongly affected in the double mutants. We consider
530 this second explanation to be more plausible, as it also might explain the synergistic
531 phenotype of the *rps24b-2 rrp7-1* and *rps24b-2 parl1-2* double mutants.

532

533 **The predominant nucleolar localization of RPS24B and its putative interactors**
534 **also support its role as an RBF**

535 Our results using the RPS24B-GFP fusion protein indicate that RPS24B is primarily
536 located in the nucleolus, with some presence in the cytoplasm; these observations are
537 consistent with previous predictions and the results of proteomic analyses. This
538 distribution reflects the dual role of RPS24B as both a structural protein of the ribosome
539 and an RBF involved in early steps of ribosome biogenesis and the transcriptional
540 repression of 45S rDNA.

541 Using different filters that included sub-organellar localization, we identified 25
542 nucleolar proteins that co-immunoprecipitated with RPS24B-GFP, which we considered
543 to be the most likely interactors. Among these were RBFs involved in the synthesis of
544 the 60S and 40S subunits, including STRS1 (AT1G31970), AT1G77030 and
545 AT3G56510, putative orthologs of yeast DBP3, DBP10 and ESF2 respectively, putative
546 ortholog of yeast, as well as NIFK. We speculate that STRS1 might also be involved in
547 repressing 45S rDNA, which would be difficult in the *rps24* background if RPS24A,
548 RPS24B, or both proteins facilitate access to the epigenetic silencing machinery at the
549 promoter of 45S rDNA. In fact, STRS1 localized with HDA2 in the nucleolus (Khan et
550 al., 2014). Like RPS6, another RP that plays extra-ribosomal roles in the maturation of

551 18S rRNA and the transcriptional regulation of 45S rDNA (Kim et al., 2014), RPS24A
552 and RPS24B might also act in this capacity.
553 We also identified At5g57120 as an RPS24B-GFP interactor. At5g57120 is the
554 putative ortholog of human NOLC1, which colocalizes with RNA Pol I in the nucleolus
555 at 47S rDNA and might activate its transcription (Chen et al., 1999). The interaction
556 between the protein encoded byAT5G57120 and RPS24B might inhibit access of the-
557 encoded protein to the 45S rDNA promoter. RPS24B, and probably RPS24A, might
558 also act as chaperones to facilitate the incorporation of RBFs into their rRNA
559 substrates, as observed for other RPs. Although we did not find SMO4 or MTR4 among
560 the RPS24B-GFP interactors, we cannot exclude the possibility that RPS24B and
561 RPS24A function in the maturation of 5.8S rRNA. However, we consider this possibility
562 unlikely, as previously argued. Interestingly, we also identified two well-known splicing
563 factors among the proteins that co-immunoprecipitated with RPS24B-GFP: PRP8 and
564 the RNA helicase BRR2. PRP8 was previously identified in a U3 snoRNA
565 ribonucleoprotein complex isolated from cauliflower (*Brassica oleracea*) inflorescences
566 (Samaha et al., 2010) and was identified in a proteomic analysis of the Arabidopsis
567 nucleolus (Palm et al., 2016). We cannot exclude the possibility that PRP8 and BRR2
568 function in ribosome biogenesis, as the expression of *RPS24B-GFP* was unable to
569 rescue the mutant phenotype of *rps24b-2* plants, suggesting that many RNA helicases
570 act in more than one pathway. Indeed, yeast Prp43p and its human ortholog DDX5 are
571 multifunctional RNA helicases that participate in ribosome biogenesis and pre-mRNA
572 splicing, among other RNA metabolic steps [reviewed in Bohnsack et al. (2022)].
573 However, our assay may have generated false positives, since expressing *RPS24B-*
574 *GFP*, which whose encoded protein we used for co-immunoprecipitation, was unable to
575 rescue the mutant phenotype of *rps24b-2* plants.
576

MATERIALS AND METHODS

Plant material and growth conditions

The wild-type Arabidopsis (*Arabidopsis thaliana*) (L) Heynh. Columbia-0 (Col-0) and Landsberg *erecta* (L*er*) accessions were provided by the Nottingham Arabidopsis Stock Centre (NASC) and propagated in our laboratory. The *api6* mutant in the L*er* background was isolated in the laboratory of J.L. Micol after ethyl methanesulfonate (EMS) mutagenesis (Berná et al., 1999). Seeds of *rps24b-2* (SALK_000766; Wang et al., 2018), *rps24a-1* (SALK_126799), *smo4-3* (SALK_071764; Micol-Ponce et al., 2018), *mtr4-2* (SAIL_50_C11; Lange et al., 2011), *rrp7-1* (SAIL_628_F08; Micol-Ponce et al., 2018) and *parl1-2* (SALK_002764; Petricka and Nelson, 2007) were also provided by NASC. Seed sterilization, sowing, plant culture and crosses were performed as previously described (Berná et al., 1999; Ponce et al., 1999).

Positional cloning of the *api6* mutation and genotyping of single and double mutants

Genomic DNA extraction and mapping of the *api6* mutation were performed as previously described (Ponce et al., 1999; 2006). The primers used for fine-mapping are listed in Supplemental Table 1. The *api6* point mutation was identified by Sanger sequencing using the primers listed in Supplemental Table 2. The presence of T-DNA insertions in *RPS24A*, *RPS24B*, *SMO4*, *RRP7, MTR4* and *PARL1* was verified by PCR using the primers shown in Supplemental Table 2.

Most Sanger sequencing reactions and electrophoreses were carried out in our laboratory with ABI PRISM BigDye Terminator Cycle Sequencing kits and an ABI PRISM 3130xl Genetic Analyzer (Applied Biosystems). Some Sanger sequencing reactions were carried out by the Stab Vida company (Portugal).

Construction of transgenic lines

The constructs used in this study were generated by Gateway cloning as described in Sánchez-García et al. (2015) using the pGEM-T Easy221 entry vector and the pMDC83 destination vector (Curtis and Grossniklaus, 2003). To generate the *35S$_{pro}$:RPS24B:GFP* transgene, the full-length coding region (without the stop codon) of *RPS24B* was amplified by PCR using genomic DNA from Col-0 as a template and primers that included the *att*B1 and *att*B2 sequences (Supplemental Table 2). The integrity of the constructs was verified by Sanger sequencing. Chemically competent *Escherichia coli* DH5α cells were transformed with the Gateway cloning products by the heat shock method, and Agrobacterium (*Agrobacterium tumefaciens*) C58C1 cells

613 were transformed by electroporation with the individual destination vectors carrying
614 each insert of interest.

615 **Plant morphological and histochemical analyses**

616 The rosettes of plants were photographed under a Nikon SMZ1500 stereomicroscope
617 equipped with a Nikon DS-Ri2 digital camera. For large rosettes, several photographs
618 from the same plant were assembled with the Photomerge tool of Adobe Photoshop
619 CS3 software (Adobe). The backgrounds of the photographs were homogenized using
620 Adobe Photoshop CS3 software without modifying the rosettes.

621 Fluorescence and confocal laser-scanning microscopy images were taken
622 under a Leica STELLARIS microscope (Leica) and processed using Leica Application
623 Suite X (LAS X) software (Leica). For nuclear staining, the roots of seedlings at 5 days
624 after stratification (das) were immersed in 0.5 µg/mL 4′,6-diamidino-2-phenylindole
625 (DAPI) for 5 min and washed two times with water. DAPI, GFP, tetramethylrhodamine-
626 5-isothiocyanate (TRITC) and cyanine 3 (Cy3) were excited at 405, 488, 503 and 506
627 nm, respectively, and their emissions collected at 425/727, 515/730, 530/732 and
628 511/726 nm, respectively.

629

630 **RT-PCR and RNA gel-blot analysis**

631 Genomic DNA was extracted from the samples using a DNeasy Plant mini kit (Qiagen)
632 from three biological replicates per genotype (leaves from a pool of three seedlings
633 collected 15 das from three different Petri plates). Total RNA was extracted from the
634 samples using TRIzol Reagent (Invitrogen) for RT-PCR and semiquantitative RT-PCR
635 and an RNeasy Plant Mini Kit (Qiagen) for RT-qPCR RNA gel blots. Three biological
636 replicates per genotype were used for RT-PCR and end-point RT-PCR, and eight were
637 used for RT-qPCR. Each biological replicate included the aerial tissues from a pool of
638 three seedlings collected 15 das from three different Petri plates. In all RT-PCR
639 assays, RNA was treated twice with Turbo DNase (Invitrogen), and reverse
640 transcription was carried out using random hexamer primers and Maxima Reverse
641 Transcriptase (Invitrogen). The *ORNITHINE CARBAMOYLTRANSFERASE* (*OTC*) and
642 *ACTIN2* (*ACT2*) housekeeping genes were used as internal controls: *OTC* for RT-PCR
643 and semiquantitative RT-PCR, and *ACT2* for RT-qPCR assays. Primers for all RT-PCR
644 assays and those used as controls for genomic DNA amplification in the analysis of
645 45S rDNA variant expression are listed in Supplemental Table 2.

646 For RNA gel-blot analysis, four digoxigenin (DIG) labeled probes were used,
647 whose sequences were obtained from Lange et al. (2011); the S6, S7 and S9 probes
648 were oligonucleotides labeled at both the 3′ and 5′ ends, synthetized by Sigma-Aldrich.
649 The S2 probe was synthetized by PCR using genomic DNA as a template, DIG-11-

650 dUTP (Roche) and the S2-Fw and S2-Rv primers (Supplemental Table 2). Two µg of
651 total RNA per sample were loaded onto 1.2% (w/v) agarose and 2.12% (v/v)
652 formaldehyde or 6% (w/v) polyacrylamide gels. Electrophoresis, hybridization and
653 detection were performed as described in Micol-Ponce et al. (2018; 2020).
654
655 **RNA-FISH and immunolocalization**
656 RNA fluorescence *in situ* hybridization (RNA-FISH) was performed as described by
657 Parry et al. (2006) and modified in Micol-Ponce et al. (2020) using the S9 probe labeled
658 with Cy3 dye (Eurofins Genomics) at a concentration of 0.5 µg/mL. Leaves were
659 mounted onto slides with Vectashield antifade mounting medium (Vector Laboratories)
660 containing 0.01 µg/mL DAPI, which was used as a nuclear marker.
661 Fibrillarin immunolocalization was performed following Pasternak et al. (2015),
662 as modified by Micol-Ponce et al. (2020). In brief, roots of seedlings were collected at 5
663 das and fixed for 40 min at 37°C in a solution containing 2% (w/v) paraformaldehyde in
664 1× microtubule-stabilizing buffer (50 mM PIPES, 5 mM $MgSO_4$, and 5 mM EGTA, pH
665 6.9) and 0.1% (v/v) Triton X-100. An anti-fibrillarin [38F3] (Abcam) primary antibody
666 was used at a 1:250 dilution, and a TRITC-conjugated anti-mouse IgG (Sigma Aldrich)
667 secondary antibody was used at a 1:500 dilution. Nuclei were stained for 10 min with
668 0.2 µg/mL DAPI and washed for 5 min before mounting the samples on slides with
669 water. Nuclei and nucleoli areas were measured as described in Micol-Ponce et al.
670 (2020) using the NIS Elements AR3.1 (Nikon) image-analysis package.
671
672 **Co-immunoprecipitation assay**
673 For co-immunoprecipitation assays, three biological replicates were used, each
674 consisting in 1 g of rosettes of *35S$_{pro}$:RPS24B:GFP* transgenic plants in the Col-0
675 background collected at 15 das. The tissue was manually ground and proteins were
676 extracted as described in Navarro-Quiles et al. (2022). Co-immunoprecipitation was
677 carried out using a µMACS GFP Isolation kit (Milteny Biotec). The effectiveness of the
678 immunoprecipitation of RPS24B-GFP was checked by immunoblotting using anti-GFP-
679 HRP antibody (Milteny Biotec).
680 The co-immunoprecipitated proteins were identified at the Centro Nacional de
681 Biotecnología (CNB) Proteomics facility (Madrid, Spain) by liquid chromatography
682 followed by tandem mass spectrometry (LC-MS/MS) using an Orbitrap Exploris 240
683 mass spectrometer. Tandem mass peptide spectra were searched against Arabidopsis
684 protein sequences in the Araport11 database using the MASCOT search engine
685 (Matrix Science). Peptide sequences identified with a false discovery rate (FDR) < 1%
686 were considered to be valid. To increase the confidence of the results, only the proteins

identified with at least two peptides in each of the three biological replicates were considered for analysis.

Accession numbers

Sequence data from this article can be found at The Arabidopsis Information Resource (https://www.arabidopsis.org/) under the following accession numbers: *RPS24A* (AT3G04920), *RPS24B* (AT5G28060), *RRP7* (AT5G38720), *SMO4* (AT2G40430), *MTR4* (AT1G59760), and *PARL1* (AT1G48920). Although AT3G04920 and AT5G28060, which encode RPS24A and RPS24B, have been renamed as ES24Z and ES24Y, respectively, according to a new nomenclature for RPs (Scarpin et al., 2022), we used their old names in this work, since the *rps24b-1* and *rps24b-2* alleles of *RPS24* were previously studied (Horiguchi et al., 2011).

FUNDING

This work was supported by grants from the Ministerio de Ciencia e Innovación of Spain (BIO2017-89728-R and PID2020-117125RB-I00 [MCI/AEI/FEDER, UE]) and the Generalitat Valenciana [PROMETEO/2019/117] to M.R.P. R.M.-P. holds a María Zambrano postdoctoral contract funded by the Next Generation EU programs and administered by the Universidad Miguel Hernández.

ACKNOWLEDGEMENTS

The authors thank F. Lozano, J. Castelló, D. Navarro and M. Gomariz for their excellent technical assistance, and J.L. Micol for useful discussions, comments on the manuscript, and providing the *api6* mutant, as well as for the use of his facilities.

AUTHOR CONTRIBUTIONS

M.R.P. obtained funding and conceived, designed and supervised research; all authors performed research and wrote the paper.

FIGURE LEGENDS

Figure 1. Alleles of the *RPS24A* and *RPS24B* genes studied in this work. (A) Schematic representation of the *RPS24B* locus, with the positions and nature of its mutations indicated. Exons and introns are depicted as black boxes and lines, respectively, and white boxes represent untranslated regions (UTRs). A red arrow and a triangle mark the point mutation of *api6* and the T-DNA insertion of *rps24b-2*, respectively. The molecular changes caused by *api6* and *rps24b-2* are shown in red in the corresponding cDNAs and predicted proteins. (B and C) Electropherograms showing the cDNA sequences of *RPS24B* in L*er* (B) and *api6* (C). Total RNA was extracted from seedlings collected 15 das. (D) Structure of the *RPS24A* gene, represented as described in A. (E-J) Rosettes of Col-0 (E), *rps24b-2* (F), *rps24a-1* (G), L*er* (H), *api6* (I) and *api6/rps24b-2* F_1 seedlings (J). Scale bars, 2 mm. Photographs were taken 14 days after stratification (das).

Figure 2. Genetic evidence for the combined haploinsufficiency of *RPS24A* and *RPS24B*. (A-D) Representative photographs of rosettes of Col-0 (A), *rps24b-2* (B), *rps24a-1* (C) and (D) *RPS24B/rps24b-2;RPS24A/rps24a-1* plants. (E-H) Siliques of (E) Col-0, (F) *rps24b-2*, (G) *rps24a-1* and (H) *RPS24B/rps24b-2;RPS24A/rps24a-1* plants. Scale bars, 2 mm (A-D), or 1 mm (E-H). Photographs were taken (A-D) at 14 or 39 (E-H) das.

Figure 3. Subcellular localization of RPS24B. (A-G) Confocal laser-scanning micrographs of root cells from transgenic *35S$_{pro}$:RPS24B:GFP* seedlings in the Col-0 background, collected at 5 das. Fluorescent signals correspond to GFP (A, C, F), 4′,6-diamidino-2-phenylindole (DAPI) (B, E), and their overlay (D, G). Scale bars, 100 µm (A), 50 µm (B-D), or 10 µm (E-G).

Figure 4. rRNA maturation in the *rps24a* and *rps24b* mutants. (A) Diagram of 45S pre-rRNA processing intermediates detected in RNA gel blots. The regions hybridizing to each probe are highlighted in green (S2 probe), yellow (S7 probe) or blue (S9 probe). Vertical bars in 45S rRNA indicate the endonucleolytic cleavage sites in pre-rRNAs that are relevant to this analysis. ETS and ITS indicate external and internal transcribed spacers, respectively. (B-D) Visualization of the processing of the 5.8S, 18S and 25S rRNA precursors by gel blot analysis. Total RNA from seedlings collected at 15 das was separated on a formaldehyde-agarose gel, transferred to a nylon membrane and hybridized with the S7 (B), S2 (C), or S9 probe (D). EtBr, ethidium bromide-stained

gels, visualized before blotting, serving as loading controls. Similar results were obtained in at least two independent experiments.

Figure 5. Genetic interactions between *rps24b-2* and mutant alleles of genes encoding RBFs. Representative photographs of rosettes of Col-0 (A), *smo4-3* (B), *mtr4-2* (C), *parl1-2* (D), *rps24b-2* (E), *rps24b-2 smo4-3* (F), *rps24b-2 mtr4-2* (G) and *rps24b-2 parl1-2* plants (H). From left to right, adult plants of Col-0 (I), *rps24b-2* (J), *smo4-3* (K), *rps24b-2 smo4-3* (L), *mtr4-2* (M), *rps24b-2 mtr4-2* (N), *parl1-2* (O) and *rps24b-2 parl1-2* (P). Photographs were taken at 21 das (A-H) or 57 das (I-P). Scale bars, 2mm (A-H), or 5 cm (I-P).

Figure 6. rRNA maturation in double mutants between *rps24b-2* and alleles of genes encoding RBFs. (A-D) Visualization of the processing of the 5.8S, 18S and 25S rRNA precursors using gel blot analysis. Total RNA from seedlings collected 15 das was separated on (A-C) formaldehyde-agarose or (D) polyacrylamide-urea gels, transferred to a nylon membrane and hybridized with the S7 (A), S2 (B), or S9 probe (C and D). EtBr, ethidium bromide-stained gels, visualized before blotting, serving as loading controls. Similar results were obtained in at least two independent experiments.

Figure 7. 45S rDNA expression in the *rps24a-1* and *rps24b-2* mutants. (A and B) Schematic representation of 45S pre-rRNA (A) and its 3′-ETS polymorphic region (B), modified from Micol-Ponce *et al.* (2018). (C and D) PCR analysis of the relative abundance of 45S rDNA variants using genomic DNA (C) and cDNA templates (D) from three biological replicates obtained from Col-0, *rps24a-1* and *rps24b-2* plants. The analysis was performed twice with similar results. (E) RT-qPCR analysis of 45S rRNA abundance. Eight biological replicates were performed per genotype (Col-0, *rps24a-1*, and *rps24b-2*), with three technical replicates in each experiment, resulting in 24 amplifications per genotype. The analyses were carried out using ExpressionSuite Software. Asterisks indicate a significant difference with Col-0 in a Mann-Whitney U test (n = 8) (*$P < 0.05$).

780 **SUPPLEMENTAL FIGURE LEGENDS**

781 **Supplemental Figure 1.** Overview of 45S pre-rRNA processing in Arabidopsis.
782 Colored boxes represent the sequences of the three mature rRNAs transcribed from
783 the 45S rDNA genes. Vertical arrows indicate endonucleolytic cleavages; letters
784 indicate the cleavage site in the corresponding pre-rRNA. Only the relevant factors and
785 the human (H) and yeast (Y) 18S pre-rRNAs related to this study are represented.
786 Based on information from Sáez-Vasquez and Delseny (2019).

787

788 **Supplemental Figure 2.** Sequence conservation between the RPS24A and RPS24B
789 paralogs. Amino acid sequence alignment of Arabidopsis RPS24B and RPS24A. The
790 14 amino acids that are absent from the RPS24B variant produced by the expression
791 of the *api6* allele are highlighted in red letters. Identical and similar residues are shaded
792 in black and gray, respectively. Asterisks and dots in the consensus line indicate
793 identical and conserved residues, respectively. Numbers indicate residue positions.
794 The alignment was obtained using ClustalW2 and shaded with Boxshade 3.21
795 (http://www.ch.embnet.org/software/BOX_form.html). Nuclear and nucleolar
796 localization sequences predicted with LOCALIZER (https://localizer.csiro.au/) and NoD
797 software (http://www.compbio.dundee.ac.uk/www-nod/index.jsp) are underlined in
798 black and green, respectively.

799

800 **Supplemental Figure 3.** *RPS24B* expression analysis. (A) Schematic representation
801 of *RPS24B* and its mutant alleles used in this study. Gene structure is represented as
802 described in the Figure 1 legend. Black arrows represent the primers used for
803 semiquantitative RT-PCR amplifications in (B). (B) Semiquantitative RT-PCR analysis
804 of *RPS24B* in the *rps24a* and *rps24b* mutants used in this study. The bands for each
805 PCR were visualized after 25, 30 and 35 cycles of amplification. Total RNA was
806 extracted from seedlings collected at 15 das. Transcripts from the *OTC* gene were
807 used as an internal control. The primer sequences used are shown in Supplemental
808 Table 1.

809

810 **Supplemental Figure 4.** Predicted localization of RPS24A. (A-B) Predicted subcellular
811 (A) and sub-organellar (B) localization of RPS24A using MULocDeep software
812 (https://mu-loc.org/).

813

814 **Supplemental Figure 5.** Predicted localization of RPS24B. (A-B) Predicted subcellular
815 (A) and sub-organellar (B) localization of RPS24B protein using MULocDeep software
816 (https://mu-loc.org/).

Supplemental Figure 6. Relative amounts of 18S and 25S RNA in the *rps24* mutants. Agilent 2100 Bioanalyzer electropherogram profiles of total RNA from Col-0, *rps24a-1*, *rps24b-2*, L*er* and *api6*. Total RNA was extracted from seedlings collected at 15 das.

Supplemental Figure 7. Genetic interactions between *rps24b-2* and *rrp7-1*. (A-D) Representative photographs of rosettes of Col-0 (A), *rps24b-2* (B), *rrp7-1* (C) and *rps24b-2 rrp7-1* plants (D). Photographs were taken from seedlings collected at 14 das. Scale bars, 2 mm.

Supplemental Figure 8. Subcellular localization of 5.8S rRNA precursors. (A-A1) RNA-FISH assay in palisade mesophyll cells from first-node leaves of L*er* (A-C), *smo4-3* (D-F), *api6* (G-I), *rps24b-2 smo4-3* (J-L), Col-0 (M-O), *mtr4-2* (P-R), *rps24a-1* (S-U), *rps24b-2 mtr4-2* (V-X) and *rps24b-2* plants (Y-A1). Fluorescent signals correspond to DAPI (in blue; A, D, G, J, M, P S, V, and Y), used as a nuclear marker; the S9 probe labeled with Cy3 (in red; B, E, H, K, N, Q, T, W, and Z); and (C, F, I, L, O, R, U, X, and A1) their overlay. Plants were collected at 21 das. Scale bars, 49 µm. (Ab and AC) Nucleus (AB) and nucleolus (AC) areas measured as DAPI and S9 probe fluorescence, respectively. Asterisks indicate significant differences from the wild type and parental lines (indicated by color) in a Student's *t*-test (*$P < 0.0001$).

Supplemental Figure 9. Nucleolus organization in *rps24* root cells. (A-I) Visualization (by immunolocalization) of the fibrillarin nuclear marker in root cells of Col-0 (A, D, and G), *rps24a-1* (B, E, and H) and *rps24b-2* plants (C, F, and I). Fluorescent signals correspond to DAPI (A-C), the secondary antibody conjugated with TRITC for fibrillarin detection (D-E) and their overlay (G-I). Immunolocalization was performed in at least 5 seedlings per genotype, collected at 5 das.

REFERENCES

Ayash M, Abukhalaf M, Thieme D, Proksch C, Heilmann M, Schattat MH, Hoehenwarter W (2021) LC-MS based draft map of the *Arabidopsis thaliana* nuclear proteome and protein import in pattern triggered immunity. Front Plant Sci **12:** 744103

Barakat A, Szick-Miranda K, Chang IF, Guyot R, Blanc G, Cooke R, Delseny M, Bailey-Serres J (2001) The organization of cytoplasmic ribosomal protein genes in the Arabidopsis genome. Plant Physiol **127:** 398-415

Berná G, Robles P, Micol JL (1999) A mutational analysis of leaf morphogenesis in *Arabidopsis thaliana*. Genetics **152:** 729-742

Bohnsack KE, Henras AK, Nielsen H, Bohnsack MT (2022) Making ends meet: a universal driver of large ribosomal subunit biogenesis. Trends Biochem Sci **48:** 213-215

Burger F, Daugeron MC, Linder P (2000) Dbp10p, a putative RNA helicase from *Saccharomyces cerevisiae*, is required for ribosome biogenesis. Nucleic Acids Res **28:** 2315-2323

Burgute BD, Peche VS, Steckelberg AL, Glockner G, Gassen B, Gehring NH, Noegel AA (2014) NKAP is a novel RS-related protein that interacts with RNA and RNA binding proteins. Nucleic Acids Res **42:** 3177-3193

Carroll AJ, Heazlewood JL, Ito J, Millar AH (2008) Analysis of the *Arabidopsis* cytosolic ribosome proteome provides detailed insights into its components and their post-translational modification. Mol Cell Proteomics **7:** 347-369

Carvalho CM, Santos AA, Pires SR, Rocha CS, Saraiva DI, Machado JP, Mattos EC, Fietto LG, Fontes EP (2008) Regulated nuclear trafficking of rpL10A mediated by NIK1 represents a defense strategy of plant cells against virus. PLOS Pathog **4:** e1000247

Casanova-Sáez R, Candela H, Micol JL (2014) Combined haploinsufficiency and purifying selection drive retention of *RPL36a* paralogs in Arabidopsis. Sci Rep **4:** 4122

Creff A, Sormani R, Desnos T (2010) The two Arabidopsis *RPS6* genes, encoding for cytoplasmic ribosomal proteins S6, are functionally equivalent. Plant Mol Biol **73:** 533-546

Curtis MD, Grossniklaus U (2003) A Gateway cloning vector set for high-throughput functional analysis of genes in planta. Plant Physiol **133:** 462-469

Chang IF, Szick-Miranda K, Pan S, Bailey-Serres J (2005) Proteomic characterization of evolutionarily conserved and variable proteins of Arabidopsis cytosolic ribosomes. Plant Physiol **137:** 848-862

Chen HK, Pai CY, Huang JY, Yeh NH (1999) Human Nopp140, which interacts with RNA polymerase I: implications for rRNA gene transcription and nucleolar structural organization. Mol Cell Biol **19:** 8536-8546

Choesmel V, Fribourg S, Aguissa-Toure AH, Pinaud N, Legrand P, Gazda HT, Gleizes PE (2008) Mutation of ribosomal protein RPS24 in Diamond-Blackfan anemia results in a ribosome biogenesis disorder. Hum Mol Genet **17:** 1253-1263

Degenhardt RF, Bonham-Smith PC (2008) Arabidopsis ribosomal proteins RPL23aA and RPL23aB are differentially targeted to the nucleolus and are disparately required for normal development. Plant Physiol **147:** 128-142

Durut N, Abou-Ellail M, Pontvianne F, Das S, Kojima H, Ukai S, de Bures A, Comella P, Nidelet S, Rialle S, Merret R, Echeverria M, Bouvet P, Nakamura K, Saez-Vasquez J (2014) A duplicated NUCLEOLIN gene with antagonistic activity is required for chromatin organization of silent 45S rDNA in Arabidopsis. Plant Cell **26:** 1330-1344

Farooq M, Lindbaek L, Krogh N, Doganli C, Keller C, Monnich M, Goncalves AB, Sakthivel S, Mang Y, Fatima A, Andersen VS, Hussain MS, Eiberg H, Hansen L, Kjaer KW, Gopalakrishnan J, Pedersen LB, Mollgard K, Nielsen H, Baig SM, Tommerup N, Christensen ST, Larsen LA (2020) RRP7A links primary microcephaly to dysfunction of ribosome biogenesis, resorption of primary cilia, and neurogenesis. Nat Commun **11:** 5816

Ferreira-Cerca S, Poll G, Gleizes PE, Tschochner H, Milkereit P (2005) Roles of eukaryotic ribosomal proteins in maturation and transport of pre-18S rRNA and ribosome function. Mol Cell **20:** 263-275

Ferreyra ML, Biarc J, Burlingame AL, Casati P (2010a) Arabidopsis L10 ribosomal proteins in UV-B responses. Plant Signal Behav **5:** 1222-1225

Ferreyra MLF, Pezza A, Biarc J, Burlingame AL, Casati P (2010b) Plant L10 ribosomal proteins have different roles during development and translation under ultraviolet-B stress. Plant Physiol **153:** 1878-1894

Fujikura U, Horiguchi G, Ponce MR, Micol JL, Tsukaya H (2009) Coordination of cell proliferation and cell expansion mediated by ribosome-related processes in the leaves of *Arabidopsis thaliana*. Plant J **59:** 499-508

Gazda HT, Grabowska A, Merida-Long LB, Latawiec E, Schneider HE, Lipton JM, Vlachos A, Atsidaftos E, Ball SE, Orfali KA, Niewiadomska E, Da Costa L, Tchernia G, Niemeyer C, Meerpohl JJ, Stahl J, Schratt G, Glader B, Backer K, Wong C, Nathan DG, Beggs AH, Sieff CA (2006) Ribosomal protein S24 gene is mutated in Diamond-Blackfan anemia. Am J Hum Genet **79:** 1110-1118

Giavalisco P, Wilson D, Kreitler T, Lehrach H, Klose J, Gobom J, Fucini P (2005) High heterogeneity within the ribosomal proteins of the *Arabidopsis thaliana* 80S ribosome. Plant Mol Biol **57:** 577-591

Hang R, Wang Z, Yang C, Luo L, Mo B, Chen X, Sun J, Liu C, Cao X (2021) Protein arginine methyltransferase 3 fine-tunes the assembly/disassembly of pre-ribosomes to repress nucleolar stress by interacting with RPS2B in *Arabidopsis*. Mol Plant **14:** 223-236

Hoang T, Peng WT, Vanrobays E, Krogan N, Hiley S, Beyer AL, Osheim YN, Greenblatt J, Hughes TR, Lafontaine DL (2005) Esf2p, a U3-associated factor required for small-subunit processome assembly and compaction. Molecular and Cell Biology **25:** 5523-5534

Horiguchi G, Fujikura U, Ferjani A, Ishikawa N, Tsukaya H (2006) Large-scale histological analysis of leaf mutants using two simple leaf observation methods: identification of novel genetic pathways governing the size and shape of leaves. Plant J **48:** 638-644

Horiguchi G, Mollá-Morales A, Pérez-Pérez JM, Kojima K, Robles P, Ponce MR, Micol JL, Tsukaya H (2011) Differential contributions of ribosomal protein genes to *Arabidopsis thaliana* leaf development. Plant J **65:** 724-736

Hruz T, Laule O, Szabo G, Wessendorp F, Bleuler S, Oertle L, Widmayer P, Gruissem W, Zimmermann P (2008) Genevestigator v3: a reference expression database for the meta-analysis of transcriptomes. Adv Bioinf **2008:** 420747

Hummel M, Dobrenel T, Cordewener JJ, Davanture M, Meyer C, Smeekens SJ, Bailey-Serres J, America TA, Hanson J (2015) Proteomic LC-MS analysis of Arabidopsis cytosolic ribosomes: Identification of ribosomal protein paralogs and re-annotation of the ribosomal protein genes. J Proteom **128:** 436-449

Jiang Y, Wang D, Yao Y, Eubel H, Kunzler P, Moller IM, Xu D (2021) MULocDeep: a deep-learning framework for protein subcellular and suborganellar localization prediction with residue-level interpretation. Comput Struct Biotechnol J **19:** 4825-4839

Kang J, Brajanovski N, Chan KT, Xuan J, Pearson RB, Sanij E (2021) Ribosomal proteins and human diseases: molecular mechanisms and targeted therapy. Signal Transduct Target Ther **6:** 323

Khan A, Garbelli A, Grossi S, Florentin A, Batelli G, Acuna T, Zolla G, Kaye Y, Paul LK, Zhu JK, Maga G, Grafi G, Barak S (2014) The Arabidopsis STRESS RESPONSE SUPPRESSOR DEAD-box RNA helicases are nucleolar- and chromocenter-localized proteins that undergo stress-mediated relocalization and are involved in epigenetic gene silencing. Plant J **79:** 28-43

Kim YK, Kim S, Shin YJ, Hur YS, Kim WY, Lee MS, Cheon CI, Verma DP (2014) Ribosomal protein S6, a target of rapamycin, is involved in the regulation of rRNA genes by possible epigenetic changes in *Arabidopsis*. J Biol Chem **289:** 3901-3912

Kojima H, Suzuki T, Kato T, Enomoto K, Sato S, Kato T, Tabata S, Sáez-Vásquez J, Echeverría M, Nakagawa T, Ishiguro S, Nakamura K (2007) Sugar-inducible expression of the nucleolin-1 gene of *Arabidopsis thaliana* and its role in ribosome synthesis, growth and development. Plant J **49:** 1053-1063

Lange H, Sement FM, Gagliardi D (2011) MTR4, a putative RNA helicase and exosome co-factor, is required for proper rRNA biogenesis and development in *Arabidopsis thaliana*. Plant J **68:** 51-63

Li S, Liu K, Zhang S, Wang X, Rogers K, Ren G, Zhang C, Yu B (2017) STV1, a ribosomal protein, binds primary microRNA transcripts to promote their interaction with the processing complex in *Arabidopsis*. Proc Natl Acad Sci USA **114:** 1424-1429

Martinez-Seidel F, Beine-Golovchuk O, Hsieh YC, Kopka J (2020) Systematic review of plant ribosome heterogeneity and specialization. Front Plant Sci **11:** 948

Mergner J, Frejno M, List M, Papacek M, Chen X, Chaudhary A, Samaras P, Richter S, Shikata H, Messerer M, Lang D, Altmann S, Cyprys P, Zolg DP, Mathieson T, Bantscheff M, Hazarika RR, Schmidt T, Dawid C, Dunkel A, Hofmann T, Sprunck S, Falter-Braun P, Johannes F, Mayer KFX, Jurgens G, Wilhelm M, Baumbach J, Grill E, Schneitz K, Schwechheimer C, Kuster B (2020) Mass-spectrometry-based draft of the Arabidopsis proteome. Nature **579:** 409-414

Micol-Ponce R, Sarmiento-Mañús R, Fontcuberta-Cervera S, Cabezas-Fuster A, de Bures A, Sáez-Vásquez J, Ponce MR (2020) SMALL ORGAN4 is a ribosome biogenesis factor involved in 5.8S ribosomal RNA maturation. Plant Physiol **184:** 2022-2039

Micol-Ponce R, Sarmiento-Mañús R, Ruiz-Bayón A, Montacié C, Sáez-Vásquez J, Ponce MR (2018) Arabidopsis RIBOSOMAL RNA PROCESSING7 is required for 18S rRNA maturation. Plant Cell **30:** 2855-2872

Montacié C, Durut N, Opsomer A, Palm D, Comella P, Picart C, Carpentier MC, Pontvianne F, Carapito C, Schleiff E, Sáez-Vásquez J (2017) Nucleolar proteome analysis and proteasomal activity assays reveal a link between nucleolus and 26S proteasome in *A. thaliana*. Front Plant Sci **8:** 1815

Navarro-Quiles C, Mateo-Bonmatí E, Candela H, Robles P, Martínez-Laborda A, Fernández Y, Simura J, Ljung K, Rubio V, Ponce MR, Micol JL (2022) The

Arabidopsis ATP-Binding Cassette E protein ABCE2 is a conserved component of the translation machinery. Front Plant Sci **13:** 1009895

Nguyen TH, Li J, Galej WP, Oshikane H, Newman AJ, Nagai K (2013) Structural basis of Brr2-Prp8 interactions and implications for U5 snRNP biogenesis and the spliceosome active site. Structure **21:** 910-919

Ni C, Buszczak M (2023) The homeostatic regulation of ribosome biogenesis. Semin Cell Dev Biol **136:** 13-26

Obayashi T, Hibara H, Kagaya Y, Aoki Y, Kinoshita K (2022) ATTED-II v11: A plant gene coexpression database using a sample balancing technique by subagging of principal components. Plant Cell Physiol **63:** 869-881

Pajerowski AG, Nguyen C, Aghajanian H, Shapiro MJ, Shapiro VS (2009) NKAP is a transcriptional repressor of notch signaling and is required for T cell development. Immunity **30:** 696-707

Palm D, Simm S, Darm K, Weis BL, Ruprecht M, Schleiff E, Scharf C (2016) Proteome distribution between nucleoplasm and nucleolus and its relation to ribosome biogenesis in *Arabidopsis thaliana*. RNA Biol **13:** 441-454

Palm D, Streit D, Shanmugam T, Weis BL, Ruprecht M, Simm S, Schleiff E (2019) Plant-specific ribosome biogenesis factors in Arabidopsis thaliana with essential function in rRNA processing. Nucleic Acids Res **47:** 1880-1895

Pan WA, Tsai HY, Wang SC, Hsiao M, Wu PY, Tsai MD (2015) The RNA recognition motif of NIFK is required for rRNA maturation during cell cycle progression. RNA Biol **12:** 255-267

Parry G, Ward S, Cernac A, Dharmasiri S, Estelle M (2006) The Arabidopsis SUPPRESSOR OF AUXIN RESISTANCE proteins are nucleoporins with an important role in hormone signaling and development. Plant Cell **18:** 1590-1603

Pasternak T, Tietz O, Rapp K, Begheldo M, Nitschke R, Ruperti B, Palme K (2015) Protocol: an improved and universal procedure for whole-mount immunolocalization in plants. Plant Methods **11:** 50

Pendle AF, Clark GP, Boon R, Lewandowska D, Lam YW, Andersen J, Mann M, Lamond AI, Brown JW, Shaw PJ (2005) Proteomic analysis of the Arabidopsis nucleolus suggests novel nucleolar functions. Mol Biol Cell **16:** 260-269

Pérez-Pérez JM, Candela H, Micol JL (2009) Understanding synergy in genetic interactions. Trends Genet **25:** 368-376

Petibon C, Malik Ghulam M, Catala M, Abou Elela S (2021) Regulation of ribosomal protein genes: an ordered anarchy. WIREs RNA **12:** e1632

Petricka JJ, Nelson TM (2007) Arabidopsis nucleolin affects plant development and patterning. Plant Physiol **144:** 173-186

Ponce MR, Robles P, Lozano FM, Brotóns MA, Micol JL (2006) Low-resolution mapping of untagged mutations. Methods Mol Biol **323:** 105-113

Ponce MR, Robles P, Micol JL (1999) High-throughput genetic mapping in *Arabidopsis thaliana*. Mol Gen Genet **261:** 408-415

Pontvianne F, Abou-Ellail M, Douet J, Comella P, Matia I, Chandrasekhara C, Debures A, Blevins T, Cooke R, Medina FJ, Tourmente S, Pikaard CS, Sáez-Vásquez J (2010) Nucleolin is required for DNA methylation state and the expression of *rRNA* gene variants in *Arabidopsis thaliana*. PLOS Genet **6:** e1001225

Pontvianne F, Matia I, Douet J, Tourmente S, Medina FJ, Echeverria M, Sáez-Vásquez J (2007) Characterization of *AtNUC-L1* reveals a central role of nucleolin in nucleolus organization and silencing of *AtNUC-L2* gene in Arabidopsis. Mol Biol Cell **18:** 369-379

Robledo S, Idol RA, Crimmins DL, Ladenson JH, Mason PJ, Bessler M (2008) The role of human ribosomal proteins in the maturation of rRNA and ribosome production. RNA **14:** 1918-1929

Sáez-Vásquez J, Delseny M (2019) Ribosome biogenesis in plants: from functional 45S ribosomal DNA organization to ribosome assembly factors. Plant Cell **31:** 1945-1967

Salih KJ, Duncan O, Li L, Trosch J, Millar AH (2020) The composition and turnover of the *Arabidopsis thaliana* 80S cytosolic ribosome. Biochem J **477:** 3019-3032

Samaha H, Delorme V, Pontvianne F, Cooke R, Delalande F, Van Dorsselaer A, Echeverria M, Saez-Vasquez J (2010) Identification of protein factors and U3 snoRNAs from a Brassica oleracea RNP complex involved in the processing of pre-rRNA. Plant J **61:** 383-398

Sánchez-García AB, Aguilera V, Micol-Ponce R, Jover-Gil S, Ponce MR (2015) Arabidopsis *MAS2*, an essential gene that encodes a homolog of animal NF-κB activating protein, is involved in 45S ribosomal DNA silencing. Plant Cell **27:** 1999-2015

Savada RP, Bonham-Smith PC (2014) Differential transcript accumulation and subcellular localization of Arabidopsis ribosomal proteins. Plant Sci **223:** 134-145

Scarpin MR, Busche M, Martinez RE, Harper LC, Reiser L, Szakonyi D, Merchante C, Lan T, Xiong W, Mo B, Tang G, Chen X, Bailey-Serres J, Browning KS, Brunkard JO (2022) An updated nomenclature for plant ribosomal protein genes. Plant Cell **35:** 640–643

Scott MS, Troshin PV, Barton GJ (2011) NoD: a nucleolar localization sequence detector for eukaryotic and viral proteins. BMC Bioinformatics **12:** 317

1064 **Schwacke R, Schneider A, van der Graaff E, Fischer K, Catoni E, Desimone M,**
1065 **Frommer WB, Flugge UI, Kunze R** (2003) ARAMEMNON, a novel database for
1066 Arabidopsis integral membrane proteins. Plant Physiol **131:** 16-26
1067 **Shanmugam T, Streit D, Schroll F, Kovacevic J, Schleiff E** (2021) Dynamics and
1068 thermal sensitivity of ribosomal RNA maturation paths in plants. J Exp Bot **72:** 7626-
1069 7644
1070 **Slavov N, Semrau S, Airoldi E, Budnik B, van Oudenaarden A** (2015) Differential
1071 stoichiometry among core ribosomal proteins. Cell Rep **13:** 865-873
1072 **Sperschneider J, Catanzariti AM, DeBoer K, Petre B, Gardiner DM, Singh KB,**
1073 **Dodds PN, Taylor JM** (2017) LOCALIZER: subcellular localization prediction of
1074 both plant and effector proteins in the plant cell. Sci Rep **7:** 44598
1075 **Tafforeau L, Zorbas C, Langhendries JL, Mullineux ST, Stamatopoulou V, Mullier**
1076 **R, Wacheul L, Lafontaine DL** (2013) The complexity of human ribosome
1077 biogenesis revealed by systematic nucleolar screening of pre-rRNA processing
1078 factors. Mol Cell **51:** 539-551
1079 **Thoms M, Thomson E, Bassler J, Gnadig M, Griesel S, Hurt E** (2015) The exosome
1080 is recruited to RNA substrates through specific adaptor proteins. Cell **162:** 1029-
1081 1038
1082 **Tyagi A, Gupta A, Dutta A, Potluri P, Batti B** (2020) A review of Diamond-Blackfan
1083 anemia: current evidence on involved genes and treatment modalities. Cureus **12:**
1084 e10019
1085 **Wang R, Zhao J, Jia M, Xu N, Liang S, Shao J, Qi Y, Liu X, An L, Yu F** (2018)
1086 Balance between cytosolic and chloroplast translation affects leaf variegation. Plant
1087 Physiol **176:** 804-818
1088 **Warner JR** (1999) The economics of ribosome biosynthesis in yeast. Trends Biochem
1089 Sci **24:** 437-440
1090 **Weaver PL, Sun C, Chang TH** (1997) Dbp3p, a putative RNA helicase in
1091 *Saccharomyces cerevisiae*, is required for efficient pre-rRNA processing
1092 predominantly at site A_3. Mol Cell Biol **17:** 1354-1365
1093 **Wilson DN, Cate JHD** (2012) The structure and function of the eukaryotic ribosome.
1094 Cold Spring Harb Perspect Biol **4:** a011536
1095 **Xiong W, Zhang J, Lan T, Kong W, Wang X, Liu L, Chen X, Mo B** (2021) High
1096 resolution RNA-seq profiling of genes encoding ribosomal proteins across different
1097 organs and developmental stages in *Arabidopsis thaliana*. Plant Direct **5:** e00320
1098 **Yang Y, Isaac C, Wang C, Dragon F, Pogacic V, Meier UT** (2000) Conserved
1099 composition of mammalian box H/ACA and box C/D small nucleolar

1100 ribonucleoprotein particles and their interaction with the common factor Nopp140.
1101 Mol Biol Cell **11:** 567-577
1102 **Zhu P, Wang Y, Qin N, Wang F, Wang J, Deng XW, Zhu D** (2016) Arabidopsis small
1103 nucleolar RNA monitors the efficient pre-rRNA processing during ribosome
1104 biogenesis. Proc Natl Acad Sci U S A **113:** 11967-11972

Cabezas-Fuster *et al*., Figure 1

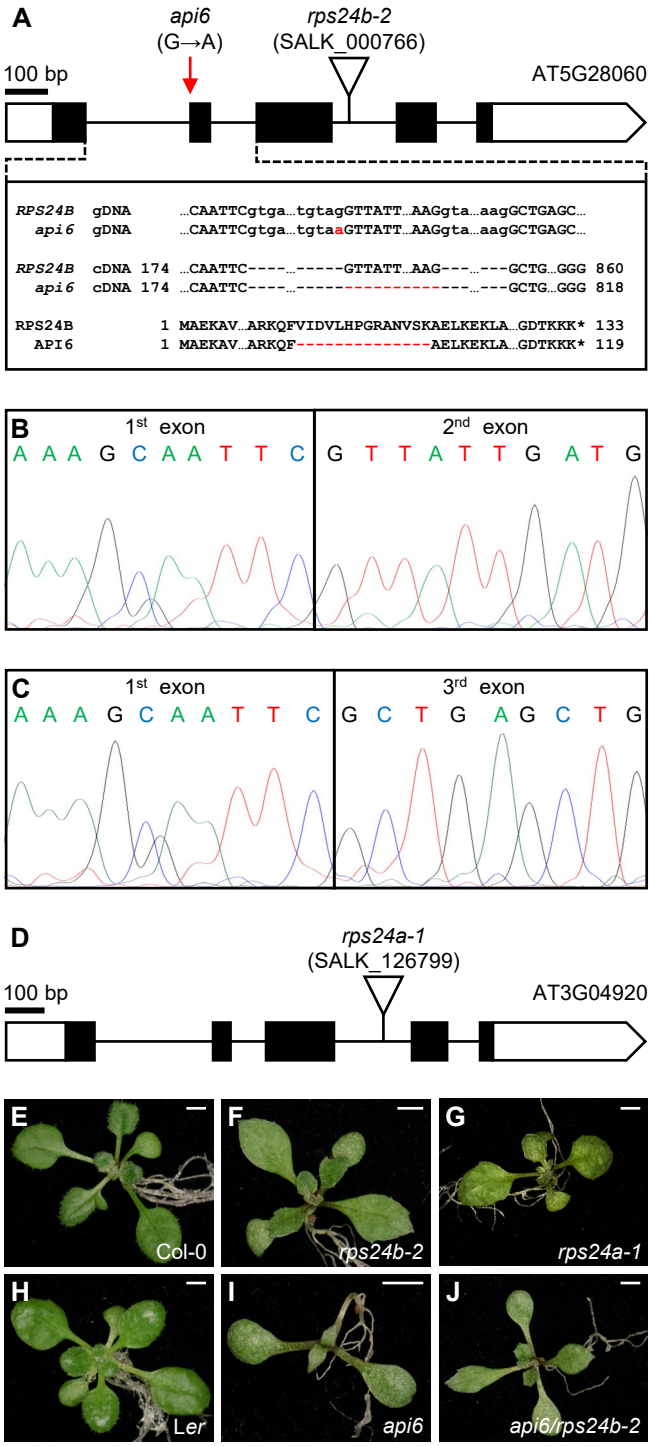

Figure 1. Alleles of the *RPS24A* and *RPS24B* genes studied in this work. (A) Schematic representation of the *RPS24B* locus, with the positions and nature of its mutations indicated. Exons and introns are depicted as black boxes and lines, respectively, and white boxes represent untranslated regions (UTRs). A red arrow and a triangle mark the point mutation of *api6* and the T-DNA insertion of *rps24b-2*, respectively. The molecular changes caused by *api6* and *rps24b-2* are shown in red in the corresponding cDNAs and predicted proteins. (B and C) Electropherograms showing the cDNA sequences of *RPS24B* in L*er* (B) and *api6* (C). Total RNA was extracted from seedlings collected 15 das. (D) Structure of the *RPS24A* gene, represented as described in A. (E-J) Rosettes of Col-0 (E), *rps24b-2* (F), *rps24a-1* (G), L*er* (H), *api6* (I) and *api6/rps24b-2* F_1 seedlings (J). Scale bars, 2 mm. Photographs were taken 14 days after stratification (das).

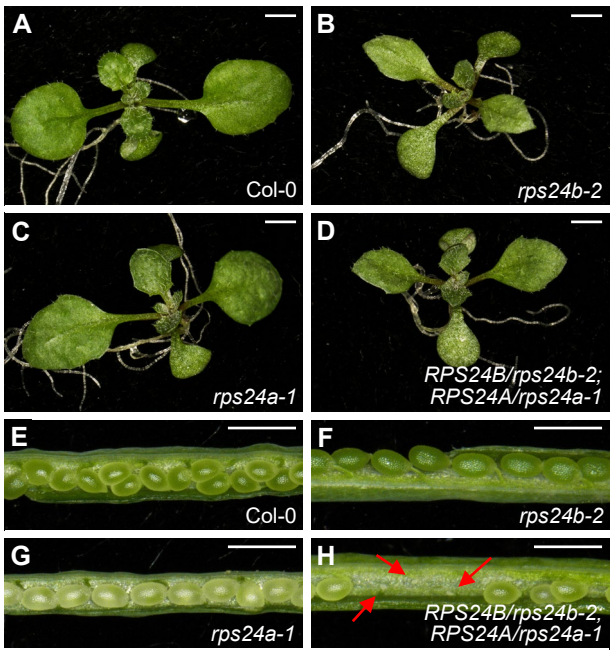

Figure 2. Genetic evidence for the combined haploinsufficiency of *RPS24A* and *RPS24B* (A-D) Representative photographs of rosettes of Col-0 (A), *rps24b-2* (B), *rps24a-1* (C) and (D) *RPS24B/rps24b-2;RPS24A/rps24a-1* plants. (E-H) Siliques of (E) Col-0, (F) *rps24b-2*, (G) *rps24a-1* and (H) *RPS24B/rps24b-2;RPS24A/rps24a-1* plants. Scale bars, 2 mm (A-D), or 1 mm (E-H). Photographs were taken (A-D) at 14 or 39 (E-H) das.

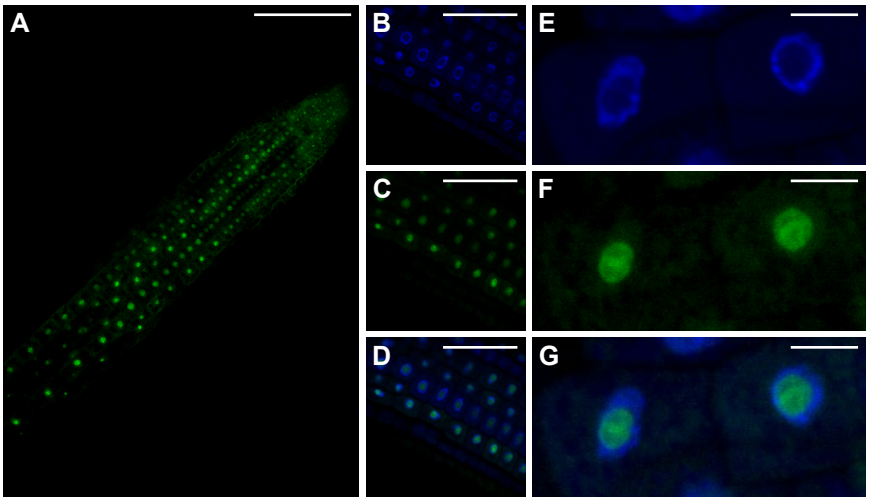

Figure 3. Subcellular localization of RPS24B. (A-G) Confocal laser-scanning micrographs of root cells from transgenic *35S$_{pro}$:RPS24B:GFP* seedlings in the Col-0 background, collected at 5 das. Fluorescent signals correspond to GFP (A, C, F), 4′,6-diamidino-2-phenylindole (DAPI) (B, E), and their overlay (D, G). Scale bars, 100 µm (A), 50 µm (B-D), or 10 µm (E-G).

Cabezas-Fuster *et al*., Figure 4

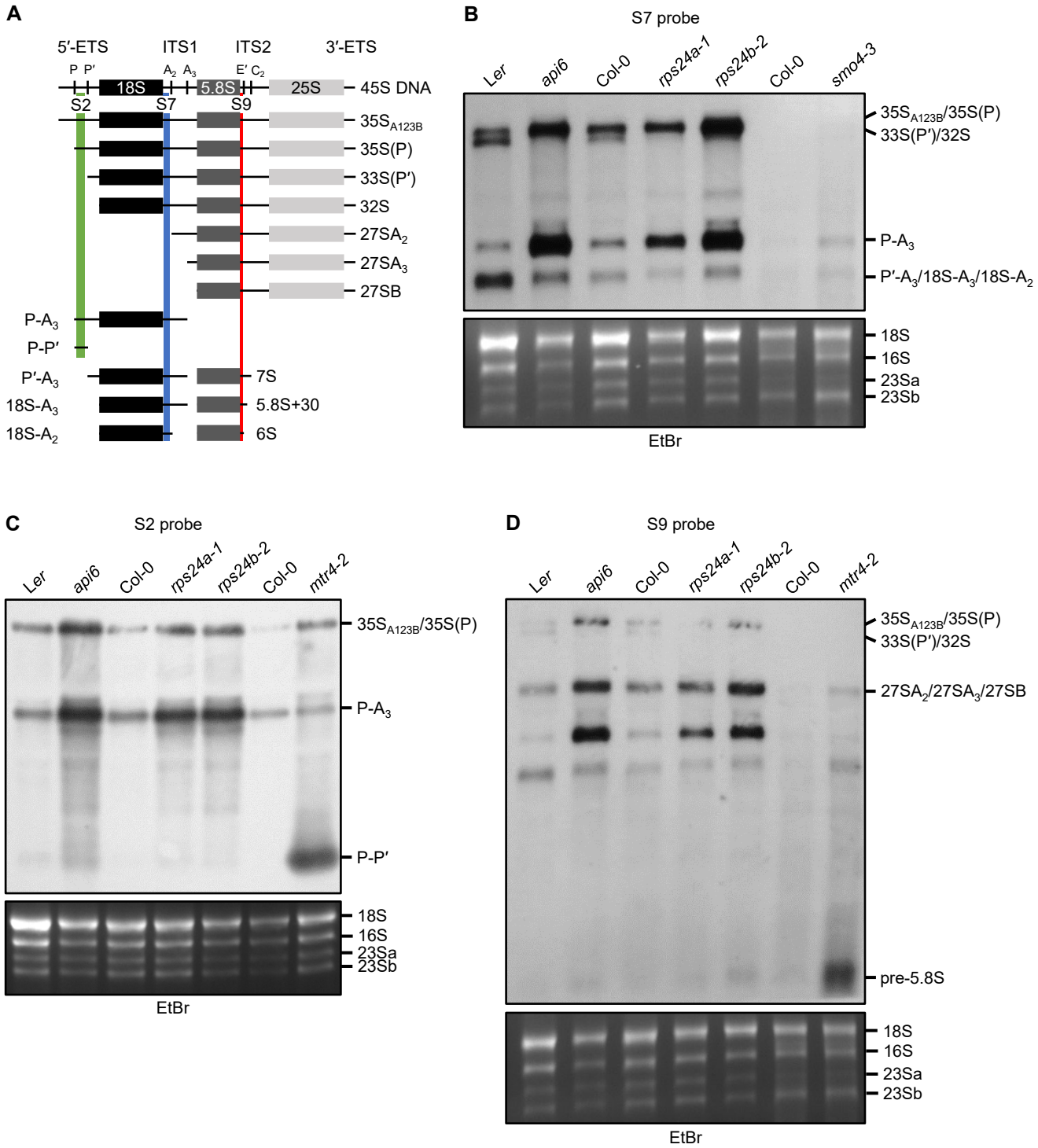

Figure 4. rRNA maturation in the *rps24a* and *rps24b* mutants. (A) Diagram of 45S pre-rRNA processing intermediates detected in RNA gel blots. The regions hybridizing to each probe are highlighted in green (S2 probe), yellow (S7 probe) or blue (S9 probe). Vertical bars in 45S rRNA indicate the endonucleolytic cleavage sites in pre-rRNAs that are relevant to this analysis. ETS and ITS indicate external and internal transcribed spacers, respectively. (B-D) Visualization of the processing of the 5.8S, 18S and 25S rRNA precursors by gel blot analysis. Total RNA from seedlings collected at 15 das was separated on a formaldehyde-agarose gel, transferred to a nylon membrane and hybridized with the S7 (B), S2 (C), or S9 probe (D). EtBr, ethidium bromide-stained gels, visualized before blotting, serving as loading controls. Similar results were obtained in at least two independent experiments.

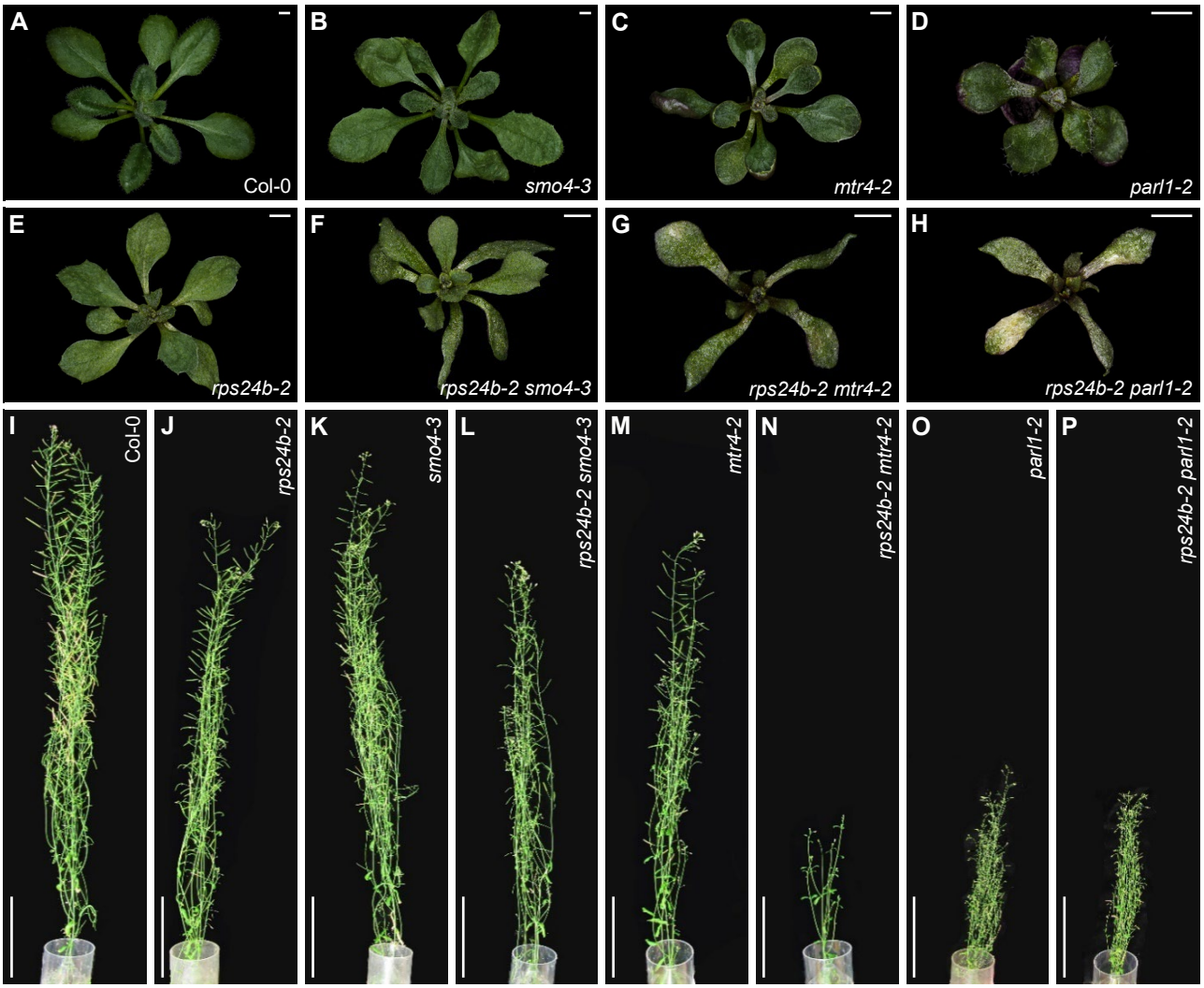

Figure 5. Genetic interactions between *rps24b-2* and mutant alleles of genes encoding RBFs. Representative photographs of rosettes of Col-0 (A), *smo4-3* (B), *mtr4-2* (C), *parl1-2* (D), *rps24b-2* (E), *rps24b-2 smo4-3* (F), *rps24b-2 mtr4-2* (G) and *rps24b-2 parl1-2* plants (H). From left to right, adult plants of Col-0 (I), *rps24b-2* (J), *smo4-3* (K), *rps24b-2 smo4-3* (L), *mtr4-2* (M), *rps24b-2 mtr4-2* (N), *parl1-2* (O) and *rps24b-2 parl1-2* (P). Photographs were taken at 21 das (A-H) or 57 das (I-P). Scale bars, 2mm (A-H), or 5 cm (I-P).

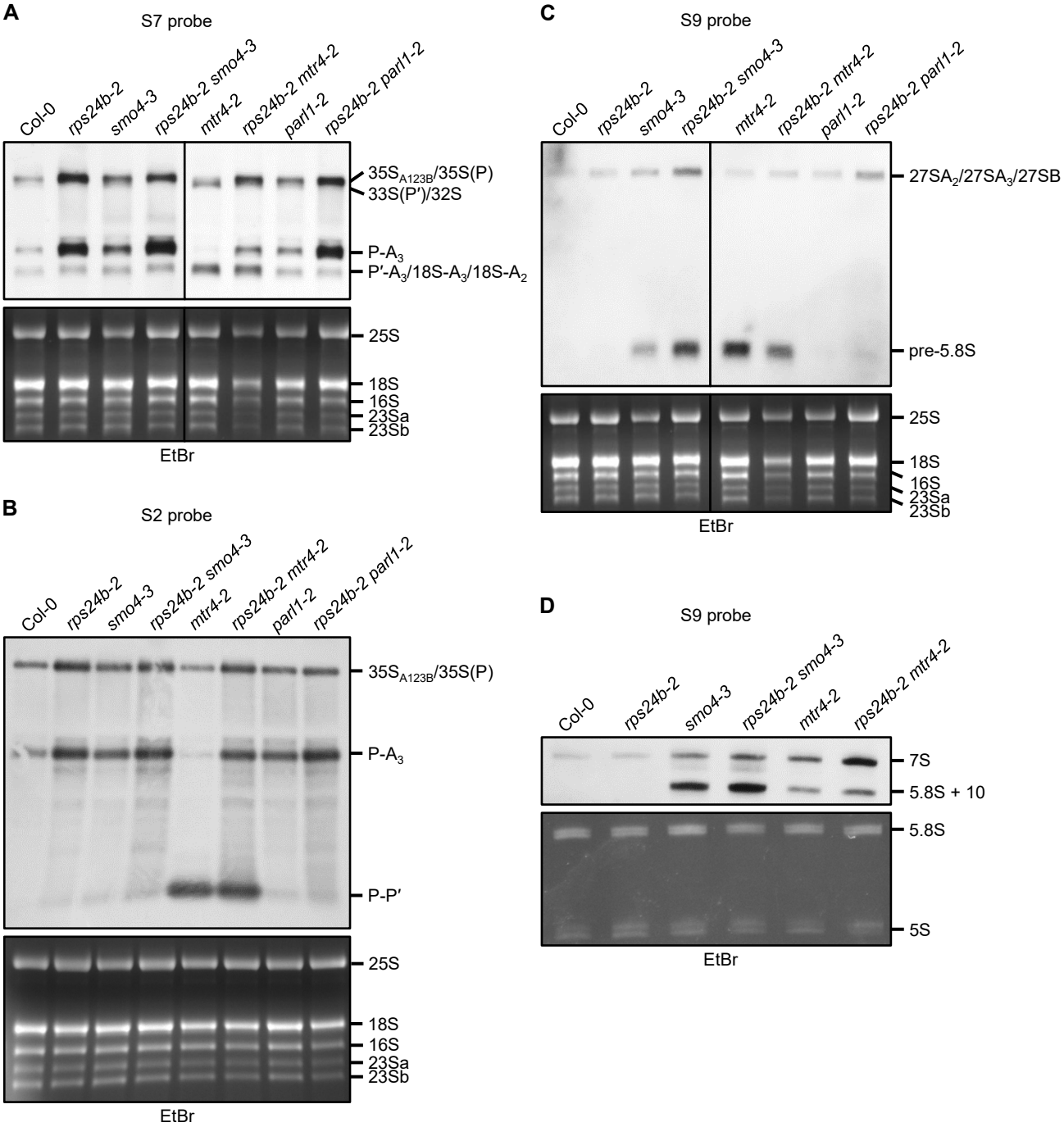

Figure 6. rRNA maturation in double mutants between *rps24b-2* and alleles of genes encoding RBFs. (A-D) Visualization of the processing of the 5.8S, 18S and 25S rRNA precursors using gel blot analysis. Total RNA from seedlings collected 15 das was separated on (A-C) formaldehyde-agarose or (D) polyacrylamide-urea gels, transferred to a nylon membrane and hybridized with the S7 (A), S2 (B), or S9 probe (C and D). EtBr, ethidium bromide-stained gels, visualized before blotting, serving as loading controls. Similar results were obtained in at least two independent experiments.

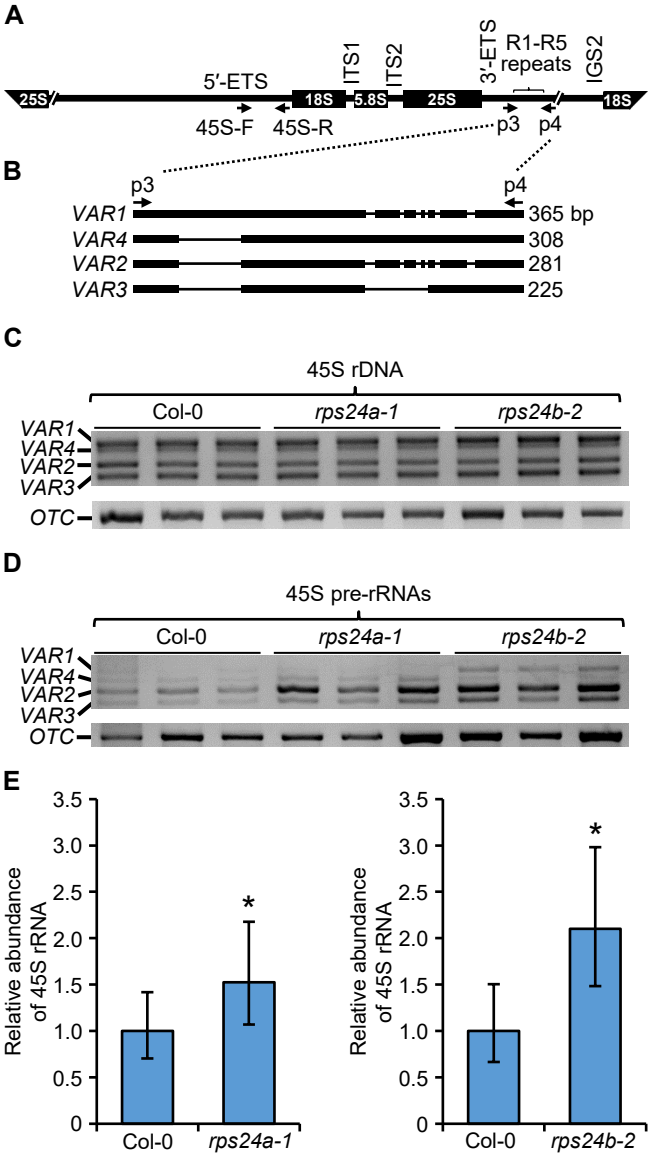

Figure 7. 45S rDNA expression in the *rps24a-1* and *rps24b-2* mutants. (A and B) Schematic representation of 45S pre-rRNA (A) and its 3′-ETS polymorphic region (B), modified from Micol-Ponce *et al.* (2018). (C and D) PCR analysis of the relative abundance of 45S rDNA variants using genomic DNA (C) and cDNA templates (D) from three biological replicates obtained from Col-0, *rps24a-1* and *rps24b-2* plants. The analysis was performed twice with similar results. (E) RT-qPCR analysis of 45S rRNA abundance. Eight biological replicates were performed per genotype (Col-0, *rps24a-1*, and *rps24b-2*), with three technical replicates in each experiment, resulting in 24 amplifications per genotype. The analyses were carried out using ExpressionSuite Software. Asterisks indicate a significant difference with Col-0 in a Mann-Whitney U test (n = 8) (*$P < 0.05$).

Parsed Citations

Ayash M, Abukhalaf M, Thieme D, Proksch C, Heilmann M, Schattat MH, Hoehenwarter W (2021) LC-MS based draft map of the Arabidopsis thaliana nuclear proteome and protein import in pattern triggered immunity. Front Plant Sci 12: 744103
Google Scholar: Author Only Title Only Author and Title

Barakat A, Szick-Miranda K, Chang IF, Guyot R, Blanc G, Cooke R, Delseny M, Bailey-Serres J (2001) The organization of cytoplasmic ribosomal protein genes in the Arabidopsis genome. Plant Physiol 127: 398-415
Google Scholar: Author Only Title Only Author and Title

Berná G, Robles P, Micol JL (1999) A mutational analysis of leaf morphogenesis in Arabidopsis thaliana. Genetics 152: 729-742
Google Scholar: Author Only Title Only Author and Title

Bohnsack KE, Henras AK, Nielsen H, Bohnsack MT (2022) Making ends meet: a universal driver of large ribosomal subunit biogenesis. Trends Biochem Sci 48: 213-215
Google Scholar: Author Only Title Only Author and Title

Burger F, Daugeron MC, Linder P (2000) Dbp10p, a putative RNA helicase from Saccharomyces cerevisiae, is required for ribosome biogenesis. Nucleic Acids Res 28: 2315-2323
Google Scholar: Author Only Title Only Author and Title

Burgute BD, Peche VS, Steckelberg AL, Glockner G, Gassen B, Gehring NH, Noegel AA (2014) NKAP is a novel RS-related protein that interacts with RNA and RNA binding proteins. Nucleic Acids Res 42: 3177-3193
Google Scholar: Author Only Title Only Author and Title

Carroll AJ, Heazlewood JL, Ito J, Millar AH (2008) Analysis of the Arabidopsis cytosolic ribosome proteome provides detailed insights into its components and their post-translational modification. Mol Cell Proteomics 7: 347-369
Google Scholar: Author Only Title Only Author and Title

Carvalho CM, Santos AA, Pires SR, Rocha CS, Saraiva DI, Machado JP, Mattos EC, Fietto LG, Fontes EP (2008) Regulated nuclear trafficking of rpL10A mediated by NIK1 represents a defense strategy of plant cells against virus. PLOS Pathog 4: e1000247
Google Scholar: Author Only Title Only Author and Title

Casanova-Sáez R, Candela H, Micol JL (2014) Combined haploinsufficiency and purifying selection drive retention of RPL36a paralogs in Arabidopsis. Sci Rep 4: 4122
Google Scholar: Author Only Title Only Author and Title

Creff A, Sormani R, Desnos T (2010) The two Arabidopsis RPS6 genes, encoding for cytoplasmic ribosomal proteins S6, are functionally equivalent. Plant Mol Biol 73: 533-546
Google Scholar: Author Only Title Only Author and Title

Curtis MD, Grossniklaus U (2003) A Gateway cloning vector set for high-throughput functional analysis of genes in planta. Plant Physiol 133: 462-469
Google Scholar: Author Only Title Only Author and Title

Chang IF, Szick-Miranda K, Pan S, Bailey-Serres J (2005) Proteomic characterization of evolutionarily conserved and variable proteins of Arabidopsis cytosolic ribosomes. Plant Physiol 137: 848-862
Google Scholar: Author Only Title Only Author and Title

Chen HK, Pai CY, Huang JY, Yeh NH (1999) Human Nopp140, which interacts with RNA polymerase I: implications for rRNA gene transcription and nucleolar structural organization. Mol Cell Biol 19: 8536-8546
Google Scholar: Author Only Title Only Author and Title

Choesmel V, Fribourg S, Aguissa-Toure AH, Pinaud N, Legrand P, Gazda HT, Gleizes PE (2008) Mutation of ribosomal protein RPS24 in Diamond-Blackfan anemia results in a ribosome biogenesis disorder. Hum Mol Genet 17: 1253-1263
Google Scholar: Author Only Title Only Author and Title

Degenhardt RF, Bonham-Smith PC (2008) Arabidopsis ribosomal proteins RPL23aA and RPL23aB are differentially targeted to the nucleolus and are disparately required for normal development. Plant Physiol 147: 128-142
Google Scholar: Author Only Title Only Author and Title

Durut N, Abou-Ellail M, Pontvianne F, Das S, Kojima H, Ukai S, de Bures A, Comella P, Nidelet S, Rialle S, Merret R, Echeverria M, Bouvet P, Nakamura K, Saez-Vasquez J (2014) A duplicated NUCLEOLIN gene with antagonistic activity is required for chromatin organization of silent 45S rDNA in Arabidopsis. Plant Cell 26: 1330-1344
Google Scholar: Author Only Title Only Author and Title

Farooq M, Lindbaek L, Krogh N, Doganli C, Keller C, Monnich M, Goncalves AB, Sakthivel S, Mang Y, Fatima A, Andersen VS, Hussain MS, Eiberg H, Hansen L, Kjaer KW, Gopalakrishnan J, Pedersen LB, Mollgard K, Nielsen H, Baig SM, Tommerup N, Christensen ST, Larsen LA (2020) RRP7A links primary microcephaly to dysfunction of ribosome biogenesis, resorption of primary cilia, and neurogenesis. Nat Commun 11: 5816

Google Scholar: Author Only Title Only Author and Title

Ferreira-Cerca S, Poll G, Gleizes PE, Tschochner H, Milkereit P (2005) Roles of eukaryotic ribosomal proteins in maturation and transport of pre-18S rRNA and ribosome function. Mol Cell 20: 263-275
Google Scholar: Author Only Title Only Author and Title

Ferreyra ML, Biarc J, Burlingame AL, Casati P (2010a) Arabidopsis L10 ribosomal proteins in UV-B responses. Plant Signal Behav 5: 1222-1225
Google Scholar: Author Only Title Only Author and Title

Ferreyra MLF, Pezza A, Biarc J, Burlingame AL, Casati P (2010b) Plant L10 ribosomal proteins have different roles during development and translation under ultraviolet-B stress. Plant Physiol 153: 1878-1894
Google Scholar: Author Only Title Only Author and Title

Fujikura U, Horiguchi G, Ponce MR, Micol JL, Tsukaya H (2009) Coordination of cell proliferation and cell expansion mediated by ribosome-related processes in the leaves of Arabidopsis thaliana. Plant J 59: 499-508
Google Scholar: Author Only Title Only Author and Title

Gazda HT, Grabowska A, Merida-Long LB, Latawiec E, Schneider HE, Lipton JM, Vlachos A, Atsidaftos E, Ball SE, Orfali KA, Niewiadomska E, Da Costa L, Tchernia G, Niemeyer C, Meerpohl JJ, Stahl J, Schratt G, Glader B, Backer K, Wong C, Nathan DG, Beggs AH, Sieff CA (2006) Ribosomal protein S24 gene is mutated in Diamond-Blackfan anemia. Am J Hum Genet 79: 1110-1118
Google Scholar: Author Only Title Only Author and Title

Giavalisco P, Wilson D, Kreitler T, Lehrach H, Klose J, Gobom J, Fucini P (2005) High heterogeneity within the ribosomal proteins of the Arabidopsis thaliana 80S ribosome. Plant Mol Biol 57: 577-591
Google Scholar: Author Only Title Only Author and Title

Hang R, Wang Z, Yang C, Luo L, Mo B, Chen X, Sun J, Liu C, Cao X (2021) Protein arginine methyltransferase 3 fine-tunes the assembly/disassembly of pre-ribosomes to repress nucleolar stress by interacting with RPS2B in Arabidopsis. Mol Plant 14: 223-236
Google Scholar: Author Only Title Only Author and Title

Hoang T, Peng WT, Vanrobays E, Krogan N, Hiley S, Beyer AL, Osheim YN, Greenblatt J, Hughes TR, Lafontaine DL (2005) Esf2p, a U3-associated factor required for small-subunit processome assembly and compaction. Molecular and Cell Biology 25: 5523-5534
Google Scholar: Author Only Title Only Author and Title

Horiguchi G, Fujikura U, Ferjani A, Ishikawa N, Tsukaya H (2006) Large-scale histological analysis of leaf mutants using two simple leaf observation methods: identification of novel genetic pathways governing the size and shape of leaves. Plant J 48: 638-644
Google Scholar: Author Only Title Only Author and Title

Horiguchi G, Mollá-Morales A, Pérez-Pérez JM, Kojima K, Robles P, Ponce MR, Micol JL, Tsukaya H (2011) Differential contributions of ribosomal protein genes to Arabidopsis thaliana leaf development. Plant J 65: 724-736
Google Scholar: Author Only Title Only Author and Title

Hruz T, Laule O, Szabo G, Wessendorp F, Bleuler S, Oertle L, Widmayer P, Gruissem W, Zimmermann P (2008) Genevestigator v3: a reference expression database for the meta-analysis of transcriptomes. Adv Bioinf 2008: 420747
Google Scholar: Author Only Title Only Author and Title

Hummel M, Dobrenel T, Cordewener JJ, Davanture M, Meyer C, Smeekens SJ, Bailey-Serres J, America TA, Hanson J (2015) Proteomic LC-MS analysis of Arabidopsis cytosolic ribosomes: Identification of ribosomal protein paralogs and re-annotation of the ribosomal protein genes. J Proteom 128: 436-449
Google Scholar: Author Only Title Only Author and Title

Jiang Y, Wang D, Yao Y, Eubel H, Kunzler P, Moller IM, Xu D (2021) MULocDeep: a deep-learning framework for protein subcellular and suborganellar localization prediction with residue-level interpretation. Comput Struct Biotechnol J 19: 4825-4839
Google Scholar: Author Only Title Only Author and Title

Kang J, Brajanovski N, Chan KT, Xuan J, Pearson RB, Sanij E (2021) Ribosomal proteins and human diseases: molecular mechanisms and targeted therapy. Signal Transduct Target Ther 6: 323
Google Scholar: Author Only Title Only Author and Title

Khan A, Garbelli A, Grossi S, Florentin A, Batelli G, Acuna T, Zolla G, Kaye Y, Paul LK, Zhu JK, Maga G, Grafi G, Barak S (2014) The Arabidopsis STRESS RESPONSE SUPPRESSOR DEAD-box RNA helicases are nucleolar- and chromocenter-localized proteins that undergo stress-mediated relocalization and are involved in epigenetic gene silencing. Plant J 79: 28-43
Google Scholar: Author Only Title Only Author and Title

Kim YK, Kim S, Shin YJ, Hur YS, Kim WY, Lee MS, Cheon CI, Verma DP (2014) Ribosomal protein S6, a target of rapamycin, is involved in the regulation of rRNA genes by possible epigenetic changes in Arabidopsis. J Biol Chem 289: 3901-3912
Google Scholar: Author Only Title Only Author and Title

Kojima H, Suzuki T, Kato T, Enomoto K, Sato S, Kato T, Tabata S, Sáez-Vásquez J, Echeverría M, Nakagawa T, Ishiguro S, Nakamura K (2007) Sugar-inducible expression of the nucleolin-1 gene of Arabidopsis thaliana and its role in ribosome synthesis, growth and development. Plant J 49: 1053-1063
Google Scholar: Author Only Title Only Author and Title

Lange H, Sement FM, Gagliardi D (2011) MTR4, a putative RNA helicase and exosome co-factor, is required for proper rRNA biogenesis and development in Arabidopsis thaliana. Plant J 68: 51-63
Google Scholar: Author Only Title Only Author and Title

Li S, Liu K, Zhang S, Wang X, Rogers K, Ren G, Zhang C, Yu B (2017) STV1, a ribosomal protein, binds primary microRNA transcripts to promote their interaction with the processing complex in Arabidopsis. Proc Natl Acad Sci USA 114: 1424-1429
Google Scholar: Author Only Title Only Author and Title

Martinez-Seidel F, Beine-Golovchuk O, Hsieh YC, Kopka J (2020) Systematic review of plant ribosome heterogeneity and specialization. Front Plant Sci 11: 948
Google Scholar: Author Only Title Only Author and Title

Mergner J, Frejno M, List M, Papacek M, Chen X, Chaudhary A, Samaras P, Richter S, Shikata H, Messerer M, Lang D, Altmann S, Cyprys P, Zolg DP, Mathieson T, Bantscheff M, Hazarika RR, Schmidt T, Dawid C, Dunkel A, Hofmann T, Sprunck S, Falter-Braun P, Johannes F, Mayer KFX, Jurgens G, Wilhelm M, Baumbach J, Grill E, Schneitz K, Schwechheimer C, Kuster B (2020) Mass-spectrometry-based draft of the Arabidopsis proteome. Nature 579: 409-414
Google Scholar: Author Only Title Only Author and Title

Micol-Ponce R, Sarmiento-Mañús R, Fontcuberta-Cervera S, Cabezas-Fuster A, de Bures A, Sáez-Vásquez J, Ponce MR (2020) SMALL ORGAN4 is a ribosome biogenesis factor involved in 5.8S ribosomal RNA maturation. Plant Physiol 184: 2022-2039
Google Scholar: Author Only Title Only Author and Title

Micol-Ponce R, Sarmiento-Mañús R, Ruiz-Bayón A, Montacié C, Sáez-Vásquez J, Ponce MR (2018) Arabidopsis RIBOSOMAL RNA PROCESSING7 is required for 18S rRNA maturation. Plant Cell 30: 2855-2872
Google Scholar: Author Only Title Only Author and Title

Montacié C, Durut N, Opsomer A, Palm D, Comella P, Picart C, Carpentier MC, Pontvianne F, Carapito C, Schleiff E, Sáez-Vásquez J (2017) Nucleolar proteome analysis and proteasomal activity assays reveal a link between nucleolus and 26S proteasome in A. thaliana. Front Plant Sci 8: 1815
Google Scholar: Author Only Title Only Author and Title

Navarro-Quiles C, Mateo-Bonmatí E, Candela H, Robles P, Martínez-Laborda A, Fernández Y, Simura J, Ljung K, Rubio V, Ponce MR, Micol JL (2022) The Arabidopsis ATP-Binding Cassette E protein ABCE2 is a conserved component of the translation machinery. Front Plant Sci 13: 1009895
Google Scholar: Author Only Title Only Author and Title

Nguyen TH, Li J, Galej WP, Oshikane H, Newman AJ, Nagai K (2013) Structural basis of Brr2-Prp8 interactions and implications for U5 snRNP biogenesis and the spliceosome active site. Structure 21: 910-919
Google Scholar: Author Only Title Only Author and Title

Ni C, Buszczak M (2023) The homeostatic regulation of ribosome biogenesis. Semin Cell Dev Biol 136: 13-26
Google Scholar: Author Only Title Only Author and Title

Obayashi T, Hibara H, Kagaya Y, Aoki Y, Kinoshita K (2022) ATTED-II v11: A plant gene coexpression database using a sample balancing technique by subagging of principal components. Plant Cell Physiol 63: 869-881
Google Scholar: Author Only Title Only Author and Title

Pajerowski AG, Nguyen C, Aghajanian H, Shapiro MJ, Shapiro VS (2009) NKAP is a transcriptional repressor of notch signaling and is required for T cell development. Immunity 30: 696-707
Google Scholar: Author Only Title Only Author and Title

Palm D, Simm S, Darm K, Weis BL, Ruprecht M, Schleiff E, Scharf C (2016) Proteome distribution between nucleoplasm and nucleolus and its relation to ribosome biogenesis in Arabidopsis thaliana. RNA Biol 13: 441-454
Google Scholar: Author Only Title Only Author and Title

Palm D, Streit D, Shanmugam T, Weis BL, Ruprecht M, Simm S, Schleiff E (2019) Plant-specific ribosome biogenesis factors in Arabidopsis thaliana with essential function in rRNA processing. Nucleic Acids Res 47: 1880-1895
Google Scholar: Author Only Title Only Author and Title

Pan WA, Tsai HY, Wang SC, Hsiao M, Wu PY, Tsai MD (2015) The RNA recognition motif of NIFK is required for rRNA maturation during cell cycle progression. RNA Biol 12: 255-267
Google Scholar: Author Only Title Only Author and Title

Parry G, Ward S, Cernac A, Dharmasiri S, Estelle M (2006) The Arabidopsis SUPPRESSOR OF AUXIN RESISTANCE proteins are nucleoporins with an important role in hormone signaling and development. Plant Cell 18: 1590-1603

Google Scholar: Author Only Title Only Author and Title

Pasternak T, Tietz O, Rapp K, Begheldo M, Nitschke R, Ruperti B, Palme K (2015) Protocol: an improved and universal procedure for whole-mount immunolocalization in plants. Plant Methods 11: 50
Google Scholar: Author Only Title Only Author and Title

Pendle AF, Clark GP, Boon R, Lewandowska D, Lam YW, Andersen J, Mann M, Lamond AI, Brown JW, Shaw PJ (2005) Proteomic analysis of the Arabidopsis nucleolus suggests novel nucleolar functions. Mol Biol Cell 16: 260-269
Google Scholar: Author Only Title Only Author and Title

Pérez-Pérez JM, Candela H, Micol JL (2009) Understanding synergy in genetic interactions. Trends Genet 25: 368-376
Google Scholar: Author Only Title Only Author and Title

Petibon C, Malik Ghulam M, Catala M, Abou Elela S (2021) Regulation of ribosomal protein genes: an ordered anarchy. WIREs RNA 12: e1632
Google Scholar: Author Only Title Only Author and Title

Petricka JJ, Nelson TM (2007) Arabidopsis nucleolin affects plant development and patterning. Plant Physiol 144: 173-186
Google Scholar: Author Only Title Only Author and Title

Ponce MR, Robles P, Lozano FM, Brotóns MA, Micol JL (2006) Low-resolution mapping of untagged mutations. Methods Mol Biol 323: 105-113
Google Scholar: Author Only Title Only Author and Title

Ponce MR, Robles P, Micol JL (1999) High-throughput genetic mapping in Arabidopsis thaliana. Mol Gen Genet 261: 408-415
Google Scholar: Author Only Title Only Author and Title

Pontvianne F, Abou-Ellail M, Douet J, Comella P, Matia I, Chandrasekhara C, Debures A, Blevins T, Cooke R, Medina FJ, Tourmente S, Pikaard CS, Sáez-Vásquez J (2010) Nucleolin is required for DNA methylation state and the expression of rRNA gene variants in Arabidopsis thaliana. PLOS Genet 6: e1001225
Google Scholar: Author Only Title Only Author and Title

Pontvianne F, Matia I, Douet J, Tourmente S, Medina FJ, Echeverria M, Sáez-Vásquez J (2007) Characterization of AtNUC-L1 reveals a central role of nucleolin in nucleolus organization and silencing of AtNUC-L2 gene in Arabidopsis. Mol Biol Cell 18: 369-379
Google Scholar: Author Only Title Only Author and Title

Robledo S, Idol RA, Crimmins DL, Ladenson JH, Mason PJ, Bessler M (2008) The role of human ribosomal proteins in the maturation of rRNA and ribosome production. RNA 14: 1918-1929
Google Scholar: Author Only Title Only Author and Title

Sáez-Vásquez J, Delseny M (2019) Ribosome biogenesis in plants: from functional 45S ribosomal DNA organization to ribosome assembly factors. Plant Cell 31: 1945-1967
Google Scholar: Author Only Title Only Author and Title

Salih KJ, Duncan O, Li L, Trosch J, Millar AH (2020) The composition and turnover of the Arabidopsis thaliana 80S cytosolic ribosome. Biochem J 477: 3019-3032
Google Scholar: Author Only Title Only Author and Title

Samaha H, Delorme V, Pontvianne F, Cooke R, Delalande F, Van Dorsselaer A, Echeverria M, Saez-Vasquez J (2010) Identification of protein factors and U3 snoRNAs from a Brassica oleracea RNP complex involved in the processing of pre-rRNA. Plant J 61: 383-398
Google Scholar: Author Only Title Only Author and Title

Sánchez-García AB, Aguilera V, Micol-Ponce R, Jover-Gil S, Ponce MR (2015) Arabidopsis MAS2, an essential gene that encodes a homolog of animal NF-κB activating protein, is involved in 45S ribosomal DNA silencing. Plant Cell 27: 1999-2015
Google Scholar: Author Only Title Only Author and Title

Savada RP, Bonham-Smith PC (2014) Differential transcript accumulation and subcellular localization of Arabidopsis ribosomal proteins. Plant Sci 223: 134-145
Google Scholar: Author Only Title Only Author and Title

Scarpin MR, Busche M, Martinez RE, Harper LC, Reiser L, Szakonyi D, Merchante C, Lan T, Xiong W, Mo B, Tang G, Chen X, Bailey-Serres J, Browning KS, Brunkard JO (2022) An updated nomenclature for plant ribosomal protein genes. Plant Cell 35: 640–643
Google Scholar: Author Only Title Only Author and Title

Scott MS, Troshin PV, Barton GJ (2011) NoD: a nucleolar localization sequence detector for eukaryotic and viral proteins. BMC Bioinformatics 12: 317
Google Scholar: Author Only Title Only Author and Title

Schwacke R, Schneider A, van der Graaff E, Fischer K, Catoni E, Desimone M, Frommer WB, Flugge UI, Kunze R (2003) ARAMEMNON, a novel database for Arabidopsis integral membrane proteins. Plant Physiol 131: 16-26
Google Scholar: Author Only Title Only Author and Title

Shanmugam T, Streit D, Schroll F, Kovacevic J, Schleiff E (2021) Dynamics and thermal sensitivity of ribosomal RNA maturation paths in plants. J Exp Bot 72: 7626-7644
Google Scholar: Author Only Title Only Author and Title

Slavov N, Semrau S, Airoldi E, Budnik B, van Oudenaarden A (2015) Differential stoichiometry among core ribosomal proteins. Cell Rep 13: 865-873
Google Scholar: Author Only Title Only Author and Title

Sperschneider J, Catanzariti AM, DeBoer K, Petre B, Gardiner DM, Singh KB, Dodds PN, Taylor JM (2017) LOCALIZER: subcellular localization prediction of both plant and effector proteins in the plant cell. Sci Rep 7: 44598
Google Scholar: Author Only Title Only Author and Title

Tafforeau L, Zorbas C, Langhendries JL, Mullineux ST, Stamatopoulou V, Mullier R, Wacheul L, Lafontaine DL (2013) The complexity of human ribosome biogenesis revealed by systematic nucleolar screening of pre-rRNA processing factors. Mol Cell 51: 539-551
Google Scholar: Author Only Title Only Author and Title

Thoms M, Thomson E, Bassler J, Gnadig M, Griesel S, Hurt E (2015) The exosome is recruited to RNA substrates through specific adaptor proteins. Cell 162: 1029-1038
Google Scholar: Author Only Title Only Author and Title

Tyagi A, Gupta A, Dutta A, Potluri P, Batti B (2020) A review of Diamond-Blackfan anemia: current evidence on involved genes and treatment modalities. Cureus 12: e10019
Google Scholar: Author Only Title Only Author and Title

Wang R, Zhao J, Jia M, Xu N, Liang S, Shao J, Qi Y, Liu X, An L, Yu F (2018) Balance between cytosolic and chloroplast translation affects leaf variegation. Plant Physiol 176: 804-818
Google Scholar: Author Only Title Only Author and Title

Warner JR (1999) The economics of ribosome biosynthesis in yeast. Trends Biochem Sci 24: 437-440
Google Scholar: Author Only Title Only Author and Title

Weaver PL, Sun C, Chang TH (1997) Dbp3p, a putative RNA helicase in Saccharomyces cerevisiae, is required for efficient pre-rRNA processing predominantly at site A3. Mol Cell Biol 17: 1354-1365
Google Scholar: Author Only Title Only Author and Title

Wilson DN, Cate JHD (2012) The structure and function of the eukaryotic ribosome. Cold Spring Harb Perspect Biol 4: a011536
Google Scholar: Author Only Title Only Author and Title

Xiong W, Zhang J, Lan T, Kong W, Wang X, Liu L, Chen X, Mo B (2021) High resolution RNA-seq profiling of genes encoding ribosomal proteins across different organs and developmental stages in Arabidopsis thaliana. Plant Direct 5: e00320
Google Scholar: Author Only Title Only Author and Title

Yang Y, Isaac C, Wang C, Dragon F, Pogacic V, Meier UT (2000) Conserved composition of mammalian box H/ACA and box C/D small nucleolar ribonucleoprotein particles and their interaction with the common factor Nopp140. Mol Biol Cell 11: 567-577
Google Scholar: Author Only Title Only Author and Title

Zhu P, Wang Y, Qin N, Wang F, Wang J, Deng XW, Zhu D (2016) Arabidopsis small nucleolar RNA monitors the efficient pre-rRNA processing during ribosome biogenesis. Proc Natl Acad Sci U S A 113: 11967-11972
Google Scholar: Author Only Title Only Author and Title